January 2013

Josephson Currents In Two-Gap Superconductor- Insulator- Superconductor Junctions

Ladan Bahrainirad

JOSEPHSON CURRENTS IN TWO-GAP SUPERCONDUCTOR-INSULATOR-SUPERCONDUCTOR JUNCTIONS

by

Ladan Bahrainirad

Bachelor of Science, Islamic Azad University, Science and research Branch, Iran, 2007

A Thesis
Submitted to the Graduate Faculty

of the

University of North Dakota

in partial fulfillment of the requirements for the degree of

Master of Science

Grand Forks, North Dakota

August

2013

This thesis, submitted by Ladan Bahrainirad in partial fulfillment of the requirements for the Degree of Master of Science from the University of North Dakota, has been read by the Faculty Advisory Committee under whom the work has been done and is hereby approved.
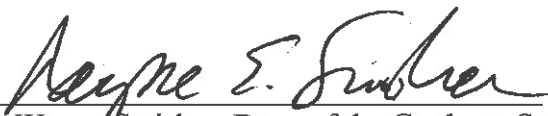
_____
Dr. Ju H.Kim Chairperson

_____
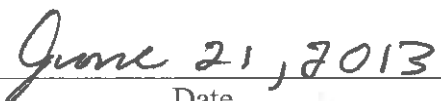Dr. Kanishka Marasinghe, Committee Member

_____
Dr. Yen Lee Loh, Committee Member

This thesis meets the standards for appearance, conforms to the style and format requirements of the Graduate School of the University of North Dakota, and is hereby approved.

_____
Dr. Wayne Swisher, Dean of the Graduate School

_____
June 21, 2013
Date

ii

PERMISSION

Title: Josephson Currents in Two-Gap Superconductor-Insulator-Superconductor Junctions

Department   Physics

Degree   Master of Science

       In presenting this thesis in partial fulfillment of the requirements for a graduate degree from the University of North Dakota, I agree that the library of this University shall make it freely available for inspection. I further agree that permission for extensive copying for scholarly purposes may be granted by the professor who supervised my thesis work or, in his absence, by the chairperson of the department or the dean of the Graduate School. It is understood that any copying or publication or other use of this thesis or part thereof for financial gain shall not be allowed without my written permission. It is also understood that due recognition shall be given to me and to the University of North Dakota in any scholarly use which may be made of any material in my thesis.

                    Ladan Bahrainirad

                    Date   6/17/2013

Table of Contents

LIST OF FIGURES

ACKNOWLEDGEMENT

I am greatly indebted to the Department of Physics of University of North Dakota for giving me wonderful opportunities during my M.S. thesis study. I would like to express my immense gratitude to my advisor Dr. Ju H. Kim, who has supervised me with enormous support and encouragement. Helpful suggestions by Dr. Yen Lee Loh had been very valuable for completion of my research. I am also grateful to my research committee member, Dr. Kanishka Marasinghe, for his guidance and insightful review.

ABSTRACT

As a way to investigate the transport property of superconductor-insulator-superconductor (SIS) junction with two-gap superconductors such as MgB_2 and iron superconductors, we study the microscopic structure of the Josephson current in a tunnel junction with a very narrow quasi-classical barrier. Also, the possibility of mid-gap states in two-gap superconductor is investigated, and their effects on the current-phase relation as well as the current density characteristics are studied. In the SIS break junction, mid-gap states appear at the Superconductor-Insulator interfaces due to an abrupt change in the superconducting order parameter, indicating that the two-gap superconductor SIS junction can yield a rich bound state structure in the energy gap. In this work, I study the mid-gap bound state energy of the two-gap superconductor-based short Josephson junctions. Also, I study the tunneling currents through the mid-gap states theoretically to estimate the effects of these bound states on the current-phase characteristics and the critical Josephson current.

CHAPTER I

INTRODUCTION

Superconductivity is a well-known macroscopic quantum phenomenon. Superconductivity was discovered by Kamerlingh Onnes in 1911 [1]. He found that mercury at a very low temperature becomes a superconductor. The phenomenon of superconductivity is characterized by the two unique properties of superconductors: i) zero resistivity and ii) Meissner effect. A superconductor provides zero resistance to the flow of electricity below a critical temperature (T_c). This property was first observed by Onnes when he placed mercury in liquid helium. He noticed that mercury has no electrical resistance below T_c at 4.15 K. Above the critical temperature (i.e., $T > T_c$), a superconductor becomes a normal metal with finite electrical resistivity. Later, Meissner and Ochsenfeld discovered that in the presence of an applied magnetic field, superconductors expel the external magnetic field. This phenomenon is known as the Meissner effect [1]. They showed that all superconductors are diamagnets because they generate an internal supercurrent to oppose the external magnetic field completely.

Based on the Meissner effect, superconductors are divided into two types: type-I and type-II superconductors. The type-I and type-II superconductors are known as the "soft" and "hard" superconductors, respectively. The type-I superconductors are mostly elemental metals in the normal state and exhibit a complete

expulsion of magnetic fields from the superconductor (i.e., Meissner effect). However, superconductivity is destroyed when the strength of external magnetic field rises above the critical magnetic field (H_c). On the other hand, most type-II superconductors are compounds or metal alloys, such as magnesium diboride and niobium-titanium. For type-II superconductors, the applied magnetic field creates a mixed state in which magnetic field lines inside the superconductor form magnetic vortices. A magnetic vortex is a normal core where magnetic field penetrates through the material. Further experiments carried out by a number of researchers revealed that superconductors revert to their normal state when either the applied current density J or the magnetic field H rises above critical current J_c (i.e., $J > J_c$) or critical field H_c (i.e., $H > H_c$), respectively.

There has been much theoretical work to explain the phenomenon of superconductivity. In 1934, Gorter and Casimir [2] proposed the two-fluid model. This model explained that superconductors have two carrier types: i) fluid of normal electrons ii) electron pairs. This model suggests that, in a superconducting material, a finite fraction of the electrons are condensed into a superfluid. Superfluid can flow through superconductors without resistance. Later, London showed that flux quantization is possible in type-II superconductors [1]. In 1950, Ginzburg and Landau formulated a phenomenological theory to study the electromagnetic and thermodynamic properties of superconductors [1]. They represented the superconducting state by using a complex order parameter. This complex order parameter is also called a quantum wave function for the superconducting state. However, these proposed models did not describe how superconductivity occurs. In 1957, Bardeen, Cooper and Schrieffer (BCS) proposed a theory [3] to explain the microscopic origin of superconductivity.

The BCS theory was the first microscopic theory of superconductivity. This theory was a good microscopic description of how electrons are interacting with lattice vibrations to yield superconductivity. However, there are many pitfalls in BCS theory, such as inability to describe the inverse isotope effect. The BCS theory is based on the idea that there is an attractive force between electrons near the Fermi level which produces weakly bound pair of electrons called Cooper pairs in superconductor. A Cooper pair has two electrons with opposite momenta and spins. At temperatures below the critical temperature T_c, this attractive force creates a new quantum state differing from the Fermi sea of a normal metal. Note that, the binding energy of a Cooper pair depends on how many other pairs have condensed and, furthermore, the center of mass motion of the pairs is so strongly correlated that each pair resides in the same state with the same center of mass motion. Due to the Fermi-Dirac statistics, the electron pairs could have less energy compared to Fermi energy. The conceptual element in this theory is the pairing of electrons close to the Fermi level into Cooper pairs through interaction with the crystal lattice. This pairing result from a slight attraction between the electrons related to lattice vibrations; the coupling to the lattice is called the electron-phonon interaction. The Cooper pairs can condense into the same level of energy like bosons.

When two or more superconductors are near each other, it may be possible for a Cooper pair to move from one superconductor to another. This motion of Cooper pair is important for understanding Josephson tunneling in superconductor junctions. In 1962, Josephson predicted the existence of tunneling current between two superconductor islands as a manifestation of macroscopic quantum phenomenon [8]. Josephson showed that the Cooper pair can tunnel from one superconductor to another through an insulator

barrier. These superconductors that are weakly linked via a tunneling barrier are also known as superconductor tunnel junctions.

1.1 Superconductor tunnel junction

Superconducting tunnel junctions are useful in microscopic device applications. One advantage of superconductor devices, as compared to the semiconductor devices, is that superconductor junctions are sensitive to voltage, current, and magnetic fields. Fabrication of a Josephson junction, involves creating a weak link between superconductors where an insulating layer is the weak-link. The insulator is a thin potential barrier which only allows electrons to tunnel through quantum mechanically. For example, a Josephson junction is made of a stack of two superconductors that are separated by a thin layer of insulator creating a superconductor-insulator-superconductor (SIS) junction. A schematic diagram of Josephson junction is shown in Fig. 1. These superconductor junctions have a wide range of applications in many fields, including electronics, physics, astrophysics, and biology. One of the most successful applications of SIS junctions is SIS heterodyne mixers. The SIS mixers may be used to detect millimeter and sub-millimeter photons. Also, the application of SIS junctions and mixers to astronomy has been very useful. For example, Caltech Sub-millimeter Observatory is using SIS junctions to explore molecular lines in interstellar clouds [34].
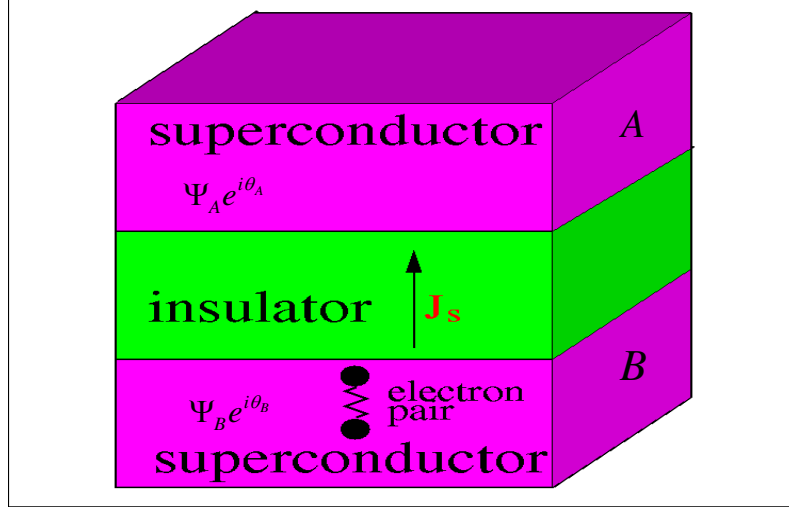
Figure 1: A superconductor-Insulator Superconductor (SIS) junction is illustrated. Cooper pair tunnel from one superconductor through the insulator to another superconductor in a single gap junction. Here, J_s denotes the tunneling current across the junction.

When the two superconductors are separated by a normal metal, instead of an insulator, we call this a superconductor-normal metal-superconductor (SNS) junction. This type of superconductor junction has a variety of applications in engineering. The SNS junction may be used in single-photon detectors for photon frequencies ranging from X-rays to infrared electromagnetic waves. In the detector, the junction is biased with a DC voltage which is less than the gap energy. When a photon is absorbed by the superconductor, it breaks a Cooper pair into two quasi-particles. The quasi-particles can tunnel across the junction in the direction of the applied voltage, indicating that the tunneling current is related to the energy of the photon.

Both SIS and SNS junctions may be classified as either long or short junctions, based on their lengths compared to a characteristic scale known as the Josephson length. The Josephson magnetic length λ_J is given by

$$\lambda_J = \sqrt{\frac{\Phi_o}{2\pi\mu_0 J_c d'}} \tag{1.1}$$

5

where μ_0 is the permeability of free space, $\Phi_o = h/2e$ is the flux quantum, J_c is the critical current density, and d' is the effective thickness of the insulator layer. If the length of the junction size L_x is greater than the Josephson length λ_J (i.e. $L_x \gg \lambda_J$), then the junction is called a long Josephson junction (LJJ). The spatial dependence of the phase difference between two adjacent superconductor layers is important for the properties of LJJs. In Fig. 2, the spatial variation of the tunneling current between two superconductor layers is indicated by arrows in the insulator layer. In the presence of a magnetic field, the phase difference depends on the vector potential which represents the magnetic flux density in the junction. It should be noted that the current variation is related to the variation in the phase difference and λ_J is specified by the externally applied magnetic field. This length scale describes the distance in which a spatial variation in the phase difference is induced. An application of a magnetic field along the insulating layer of a single LJJ induces magnetic vortices, which are also called Josephson vortices.
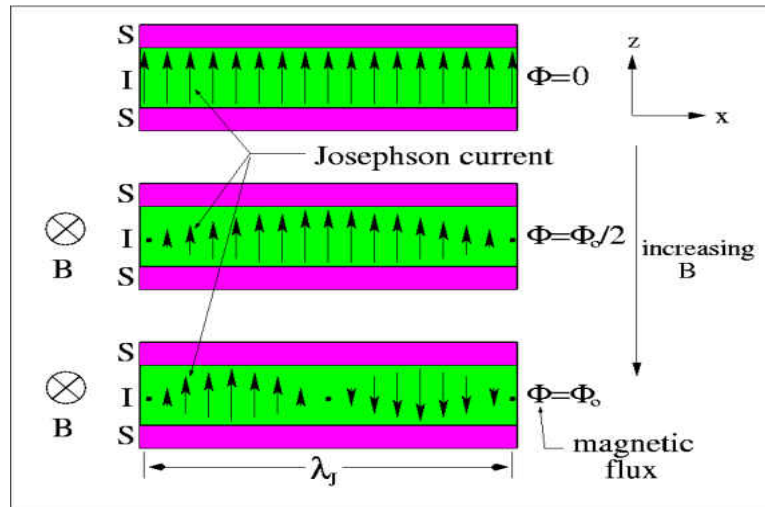
Figure 2: The effect of magnetic field on the tunneling current in a uniform Long Josephson junction is depicted. Arrows illustrate the strength and the direction of the Josephson current.

LJJs are good candidates for generating high-frequency electromagnetic radiation. Among many applications of the LJJ, terahertz (THz) radiation generator by using high-T_c cuprates is one of the well-known examples. In the THz radiation application, the frequency of emission is tunable by the voltage across the device. THz radiation may be applied in many fields like recognizing protein structural states [4], visualizing and cataloging absorption and contrast mechanisms in tissue [5, 6], radiation effects on biological samples , biological processes, and diagnose the diseases [7].

On the other hand, if the size of the junction L_X is much smaller than the Josephson length λ_J (i.e., $L_X << \lambda_J$), then the junction is called a short Josephson junction (SJJ). The SJJ has many different applications. A superconducting quantum interference device (SQUID) is one of the most important applications. This device, which was invented by Jaklevic, Lambe, and Mercereau [35], and Arnold Silver, may be used as a very sensitive magnetometer to measure a very weak magnetic field of order of 10^{-15} Tesla. This range of sensitivity is useful in many fields including biology, physics, and medicine. The SQUID, as shown schematically in Fig. 3, consists of two superconductors separated by thin insulator. The central element of a SQUID is a loop of superconductor with one or more weak links. In this system there is a superconducting ring where one or two small piece of insulator is inserted from the ring.
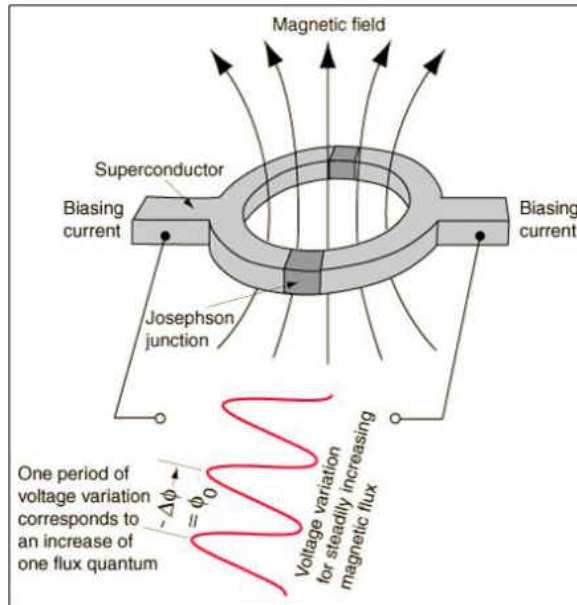
Figure 3: A SQUID consists of two superconductors separated by thin layers of insulator, forming two parallel Josephson junctions. Parallel Josephson junctions are used in SQUID devices for the detection of very weak magnetic fields.

1.2 Josephson Effect

Josephson effect is an example of a macroscopic quantum phenomenon and is one of the important fundamental phenomena in condensed matter physics. In 1962, Josephson made a remarkable prediction that two superconductors separated by a thin insulating barrier should give rise to a spontaneous current [8]. Josephson discovered the possibility of pair tunneling between two superconductors. He found that Cooper pairs of electron can tunnel through the barrier and carry a current, at zero voltage bias. There are two main effects predicted by Josephson: (1) DC Josephson effect and (2) AC Josephson effect [8].

Josephson predicted that the Cooper pairs can tunnel across an insulating barrier, causing a current, without any externally applied potential difference (i.e., V = 0). This phenomenon of appearance of tunneling current in the absence of a bias voltage is known

as the DC Josephson effect. The DC Josephson effect accounts for the relationship between the tunneling current and the phase difference between two superconductor islands. A DC tunneling current flows through the insulator in the junction. The Josephson current density is given by

$$J = J_c \sin \varphi \qquad (1.2)$$

where J_c is the Josephson critical current density and $\varphi = \theta_2 - \theta_1$ is the phase difference between the order parameters of the two superconductor layers. Note that θ is the phase of the superconducting order parameter which can be defined as

$$\psi(r) = |\psi| e^{i\theta} \qquad (1.3)$$

where $|\psi|$ is the amplitude which is related to the number of superelectrons. This effect also indicates a nonlinear dependence on the phase difference of the current flow across the junction in the absence of bias voltage.

The AC Josephson effect explains the temporal variation of the phase difference with applied voltage. While a voltage V is applied through the junction, the phase difference between superconductor changes since the electron pairs experiences a potential difference 2eV across the junction. In this case, it is found that the electron pairs oscillate across the junction, with a frequency given by

$$\frac{\partial \phi}{\partial t} = \frac{2eV}{\hbar} \qquad (1.4)$$

where e is the electronic charge and $\hbar = h/2\pi$, and h is the Planck's constant. This relationship indicates that an electromagnetic wave with energy $\hbar\omega = 2eV$ can be either emitted or absorbed as an electron pair oscillates across the barrier. Hence, the Josephson current oscillates with the frequency $\omega = 2\pi V/\hbar$. In Fig. 4, a typical current-voltage (I-

V) characteristic of the Josephson junction is shown schematically. When the voltage is applied, Cooper pairs oscillate back and forth across the junction. However the Cooper pair does not break till the applied voltage is larger than a threshold value. Since the binding energy of the Cooper pair is 2Δ where Δ is the superconducting energy gap per electron, the minimum voltage needed to break up a Cooper pair into quasi-particles is $2\Delta/e$.
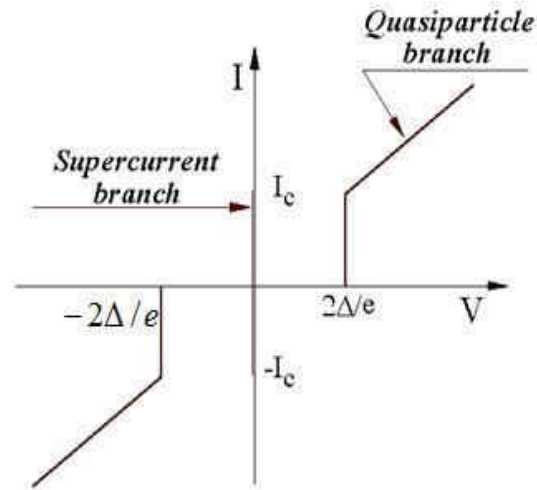
Figure 4: A current-voltage (I-V) characteristic of a superconductor tunnel junction is shown schematically. Here, $2\Delta/e$ represents the gap voltage of the junction. I_c denotes the Josephson critical current.

In predicting the presence of tunneling current in a Josephson junction, Josephson applied quantum mechanics by using a macroscopic wave function to represent the superconducting state. He used the time-independent Schrödinger equation to deal with coherent transmission of Cooper pairs through a tunnel barrier. However, a microscopic understanding for the origin of tunneling was not complete. In 1991, Furusaki and Tsukada [10] developed the microscopic approach by examining an SNS junction by treating it as a quantum mechanical scattering problem. Furusaki and Tsukada

introduced the microscopic structure of the Josephson current in a SNS tunnel junction with a wide quasi-classical tunnel barrier and predicted that mid-gap states, which are localized near the edges or in the middle of gaps, carry the current through the junction.

The remainder of the thesis is organized as follows. In Chapter II, I present the microscopic origin of the mid-gap states in one-gap superconductor tunnel junction by using Bogoliubov-de Gennes equations. In Chapter III, I describe the BCS model for a two-gap superconductor and discuss features that are important for Josephson junctions. In Chapter IV, I explain the origin of mid-gap states at a two-gap superconductor-normal metal interface by examining Andreev reflection. In Chapter V, I calculate the energies of the mid-gap states for an SIS break junction involving two-gap superconductors. Finally, I summarize the result of the present thesis and conclude in Chapter VI.

CHAPTER II

INTERFACE OF NORMAL METAL AND ONE-GAP SUPERCONDUCTOR

In this chapter, I discuss the physics of a normal metal-superconductor (NS) interface of one-gap superconductor by using the theory proposed by Blonder, Tinkham, and Klapwijk (BTK). This is known as BTK theory. I outline the physics of the process when an electron falls onto the NS interface based on the work by Tinkham and Blonder [9]. Within the context of the BTK theory, I discuss the current-voltage (I−V) characteristics of NS interface involving one-gap superconductor. One important advantage of the BTK theory is its applicability to a wide range of NS interfaces. The theory describes the junction by introducing a barrier potential of an arbitrary strength at the interface. To determine the transmission and reflection of the quasi-particles at the interface, the BTK theory utilizes the Bogoliubov-de Gennes equations.

2.1 Bogoliubov-de Gennes equation

In this section, I discuss the Bogoliubov-de Gennes (BdG) equations. Using the solution of these equations, I construct the wave function for a superconducting system which is used in the BTK theory. The BdG equations are the mean-field equations for

the superconducting system. These equations are obtained as the equations of motion by making the mean-field approximation to the BCS Hamiltonian.

To describe the superconducting state by using the BCS theory, I start with the BCS Hamiltonian which is written as

$$H_{BCS} = \sum_{k\sigma} \varepsilon_k c_{k\sigma}^+ c_{k\sigma} - \sum_{kk'} V_{kk'} \cdot c_{k\uparrow}^+ c_{-k\downarrow}^+ c_{-k'\downarrow} c_{k'\uparrow} \tag{2.1}$$

where $V_{kk'}$ the pairing matrix which accounts for the effective interaction between electrons. The matrix element $V_{kk'}$, in general, depends on the nature of interaction yielding effective attraction between the electrons, but I simplify it by making the mean-field approximation. Here, $\varepsilon_k = (\hbar^2 k^2/2m) - \mu$ denotes the kinetic energy and μ is the chemical potential. The fermion operators $c_{k\sigma}^+$ and $c_{k\sigma}$ represent creation and annihilation of an electron, respectively. I note that k and σ represent the momentum and spin variable, respectively. These fermion annihilation and creation operators obey the anti-commutation rules

$$\{c_{k\sigma}^+, c_{k\sigma}\} = c_{k\sigma}^+ c_{k\sigma} + c_{k\sigma} c_{k\sigma}^+ = \delta_{kk'} \delta_{\sigma\sigma'} \tag{2.2}$$

and

$$\{c_{k\sigma}^+, c_{k\sigma}\} = \{c_{k\sigma}^+, c_{k'\sigma'}^+\} = 0 \tag{2.3}$$

I can obtain the energy spectrum from the BCS model of Eq. (2.1) by making the mean-field approximation. By employing the Wick's theorem to reduce the two-body interaction term into effective one-body terms, I approximate the second term of the Eq. (2.1) as

$$-\sum_{kk'} V_{kk'} \cdot c_{k\uparrow}^+ c_{k\downarrow}^+ c_{-k'\downarrow} c_{k'\uparrow} \Rightarrow -\sum_{kk'} V_{kk'} \left(\left\langle c_{k\uparrow}^+ c_{-k\downarrow}^+ \right\rangle c_{-k'\downarrow} c_{k'\uparrow} + \left\langle c_{-k'\downarrow} c_{k'\uparrow} \right\rangle c_{k\uparrow}^+ c_{-k\downarrow}^+ \right) \tag{2.4}$$

13

Here, I define the pairing parameter as

$$\Delta_k = -\sum_{k'} V_{kk'} \langle c_{-k'\downarrow} c_{k'\uparrow} \rangle \tag{2.5}$$

This order parameter is zero ($\Delta = 0$) in the normal state and non-zero ($\Delta \neq 0$) in the superconducting state. In this mean-field theory, I rewrite the model Hamiltonian of Eq. (2.1) as

$$H_{BCS} = \sum_k \varepsilon_k c_{k\sigma}^+ c_{k\sigma} - \sum_{kk'} V_{kk'} \left(\Delta^* c_{-k'\downarrow} c_{k'\uparrow} + \Delta c_{k\uparrow}^+ c_{-k\downarrow}^+ \right) \tag{2.6}$$

The mean-field Hamiltonian H_{BCS} may be diagonalized by using a rotational transformation known as the Bogoliubov transformation [9]. The Bogoliubov transformation is specified as

$$c_{k\uparrow} = u_k^* \xi_k + v_k \xi_k^* \tag{2.7}$$

$$c_{-k\uparrow} = -v_k^* \xi_k + u_k \xi_k^* \tag{2.8}$$

where the coefficients u_k and v_k represent the coherence factor for the particles and holes, respectively. These coefficients satisfy the condition

$$|u_k|^2 + |v_k|^2 = 1 \tag{2.9}$$

Note that the fermion operator ξ_k is the rotational transformation, participates in destroying an electron with $k\uparrow$ and creating with $-k\downarrow$. Therefore, the momentum of the system will decrease by $\hbar/2$. The parameter ξ_k^* has the same property.

The excitation spectrum of quasi-particles in the superconducting state can be described by the BdG equations. The BdG equations are written as

$$H_{BdG}\psi = E\psi \tag{2.10}$$

where the Hamiltonian H_{BdG} is given by

$$H_{BdG} = \begin{pmatrix} \varepsilon(r,r') & \Delta(r,r') \\ \Delta^*(r,r') & -\varepsilon^*(r,r') \end{pmatrix} \tag{2.11}$$

The wave function ψ has two components which is given by

$$\psi_k(r) = \begin{pmatrix} u_k(r) \\ v_k(r) \end{pmatrix} \tag{2.12}$$

where u_k and v_k describe the electron and hole excitation, respectively. The BdG Hamiltonian has the 'particle-hole' symmetry. The BdG equation has both positive and negative energy solutions

$$E = \pm\sqrt{\Delta^2 + \varepsilon_k^2} \tag{2.13}$$

I note that, in the ground state, the negative energy levels are below the Fermi energy and are filled, while the positive energy levels are above the Fermi energy and are empty. Excitation of a particle represents destruction of a particle in a state with negative energy and creation of a particle in a state with positive energy. The two-component solutions are

$$u_k^2 = \frac{1}{2}\left(1 + \frac{\sqrt{E^2 - \Delta^2}}{E}\right) \tag{2.14}$$

and

$$v_k^2 = \frac{1}{2}\left(1 - \frac{\sqrt{E^2 - \Delta^2}}{E}\right) \tag{2.15}$$

These solutions represent the wave function for electrons and holes in the superconductor.

2.3 Andreev reflection and Andreev bound state

Now, I consider the Andreev reflection at the NS interface. The Andreev reflection is a type of particle scattering which occurs at the interfaces between a superconductor (S) and normal metal (N) as shown in Fig. 5. The process involves an electron incident on the interface from the normal metal side being reflected as a hole on the same side.
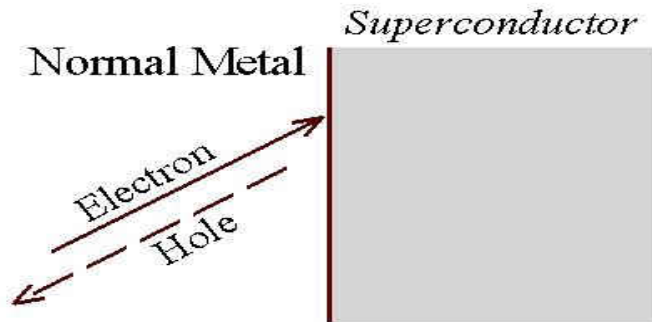
Figure 5: The NS junction is illustrated. The Andreev retro-reflection at the NS interface has been shown schematically.

The Andreev reflection is a process in which the incoming electron gets reflected as a hole on the normal metal side, a Cooper pair gets transmitted to the superconductor side as shown Fig. 6. This reflection arises as part of particle-hole creation: a hole is returned by the Andreev reflection while a particle forms a Cooper pair with the incident electron in the superconductor, as shown in Fig. 6. Note that, the Andreev reflection is an elastic collision; therefore, the energy is conserved in the process.
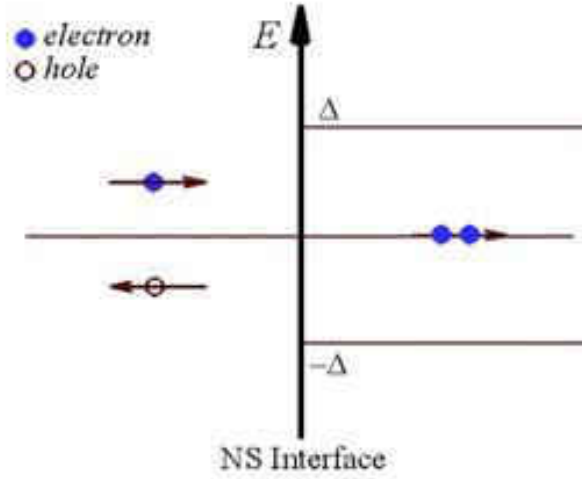
Figure 6: A schematic diagram illustrating Andreev reflection at a NS interface. Here, N and S indicate normal, superconductor region respectively. The blue circles are shown the electron in both sides while the other one present the hole. An electron comes from N side and while leaves an hole in the same side it will construct a Cooper pair with another electron in the S side.

As shown in Fig. 6, the Andreev reflection appears as a conversion of a particle into a hole. I note that energy of the incident particle is less than the gap energy (i.e., $E < \Delta$) at zero temperature. An incoming electron has momentum k_+, and a Cooper pair is formed with another electron with opposite momentum k_-. Hence, these two electrons form a Cooper pair. The pairing electron comes from the N side and leaves a hole with momentum k_-. So, I define the energy of these electron and hole branches as

$$\frac{\hbar k_{\pm}}{2m} = \mu \pm \sqrt{E^2 - \Delta^2} \qquad (2.16)$$

In this charge-transfer process, the normal current in N is converted to supercurrent in S. Each Andreev reflection transfers a charge 2e across the interface, avoiding the forbidden single-particle transmission within the superconducting energy gap. In this process, instead of a charge e, a charge of 2e is transported across the interface, and consequently the resistance has decreased by a factor of 2. The energy is conserved in the process

since the Cooper pair has $2E_F$. The incoming electron with energy $E_F + E$ and the reflected hole with energy $E_F - E$ yield the total energy of $2E_F$. Theoretical description of the conductance of electrons and holes is provided by the BTK theory.

2.4 NS interface: BTK model

The BTK theory explains the tunneling process between a normal metal and a conventional s-wave superconductor [9] by consider it as a potential scattering problem. The solution to the BdG equations for superconductor in Sec 2.1 is the starting base for the BTK theory. The BdG equations describe the BCS theory for superconductors with spatially dependent pairing strength $\Delta(x)$. A SN interface may be described by the time-independent Schrödinger equations which is given by

$$\begin{bmatrix} -\dfrac{\hbar^2}{2m}\dfrac{\partial^2}{\partial x^2} - \mu + V(x) & \Delta(x) \\ \Delta^*(x) & \dfrac{\hbar^2}{2m}\dfrac{\partial^2}{\partial x^2} + \mu - V(x) \end{bmatrix} \begin{bmatrix} u(x) \\ v(x) \end{bmatrix} = E \begin{bmatrix} u(x) \\ v(x) \end{bmatrix} \qquad (2.17)$$

where $\mu(x)$ is the chemical potential. Here, I assume that $\Delta(x)$, $\mu(x)$, and $V(x)$ are constant. Also, I use a delta-function potential $V = \Lambda\delta(x)$ to describe the potential at the boundary, related to the resistance of the interface. The wave function has two components which are given by

$$\psi_k(x) = \begin{bmatrix} u_k(x,t) \\ v_k(x,t) \end{bmatrix} \qquad (2.18)$$

Then, I solve the BdG equations for the superconductor and normal metal side, separately. I note that $\Delta(x) = 0$ for the normal side. An incident electron from the normal metal side, it can be reflected as a hole. The incident electron is transmitted as a

Cooper pair. The solutions to the BdG equations suggest that the wave function for the normal metal side has two contributions due to propagation of hole and electron waves. The wave function on the normal side is

$$\Psi_N(x) = \begin{bmatrix} 1 \\ 0 \end{bmatrix} e^{ik_+x} + a \begin{bmatrix} 0 \\ 1 \end{bmatrix} e^{ik_-x} + b \begin{bmatrix} 1 \\ 0 \end{bmatrix} e^{-ik_+x} \tag{2.19}$$

Similarly, by using the solutions of BdG equations for $\Delta \neq 0$, I construct the wave function for the superconductor side as

$$\Psi_S^t(x) = c \begin{bmatrix} u_{k_F} \\ v_{k_F} \end{bmatrix} e^{ik_+x} + d \begin{bmatrix} v_{k_F} \\ u_{k_F} \end{bmatrix} e^{-ik_-x} \tag{2.20}$$

where k_F is the Fermi vector. The coefficients a, b, c, and d in Eqs. (2.18) and (2.19) can be determined by apply the boundary conditions. I apply the usual two boundary conditions: the wave functions are i) continuous and ii) smooth. The continuity of wave function at the interface is given by

$$\Psi_N(0) = \Psi_S(0) = \Psi(0) \tag{2.21}$$

The smoothness of the wave functions, represented as the derivative of the wave functions, satisfies the condition

$$\frac{\hbar^2}{2m} \frac{d\Psi_S(0)}{dx} - \frac{\hbar^2}{2m} \frac{d\Psi_N(0)}{dx} = \Lambda\Psi(0) \tag{2.22}$$

The probability current density J_p can be calculated at the NS interface. In general, the current density J_p is expressed as

$$J_p = \frac{\hbar}{m} \text{Im}[u^*(x)\nabla u(x) - v^*(x)\nabla v(x)] \tag{2.23}$$

Here, "Im" means the imaginary part. The current density J_N in the normal metal side can be written as

$$J_N = v_f(1 - a^2 - b^2) \qquad (2.24)$$

Similarly, the current density J_S in the superconductor side can be written as

$$J_S = v_f \left(|u_0|^2 - |v_0|^2 \right)\left(|c|^2 + |d|^2 \right) \qquad (2.25)$$

All the incident particles convert into the reflected and transmitted particles and holes. This condition requires that $J_N = J_S$ and yields the relation

$$(1 - a^2 - b^2) = \left(|u_0|^2 - |v_0|^2 \right)\left(|c|^2 + |d|^2 \right) \qquad (2.26)$$

The above expressions for the probability current densities enabled BTK to derive the current-voltage relation [9]. Consequently, when a bias voltage is applied, the total current flowing from normal electrode to the superconductor is given by

$$I = \frac{2e^2}{\hbar} \int dE\, T(E)[f(E - eV) - f(E)] \qquad (2.27)$$

where $T(E) = 1 - B(E) + A(E)$ denotes the transmission coefficient, and $f(E)$ is the Fermi-Dirac distribution function. In Eq. (2.12), for $E > \Delta$, the coefficients Andreev reflection $A(E)$ and normal reflection $B(E)$ are given by

$$A(E) = a^2 = \frac{u_{k_F}^2 v_{k_F}^2}{\rho^2} \qquad (2.28)$$

and

$$B(E) = b^2 = \frac{(u_{k_F}^4 + v_{k_F}^4 - 2u_{k_F}^2 v_{k_F}^2)z^2(1 + z^2)}{\rho^2} \qquad (2.29)$$

where the dimensionless parameter $z = m\Lambda/\hbar^2 k_F$ accounts for the strength of the barrier at the interface, and the dimensionless parameter ρ is given by

$$\rho = u_{k_F}^2 + \frac{(u_0^2 + v_0^2)}{z^2} \qquad (2.30)$$

20

However, for $E < \Delta$, these parameter may defined differently such as

$$A(E) = a^2 = \frac{\Delta^2}{E^2 + (\Delta^2 - E^2)(1 + 2z^2)} \qquad (2.31)$$

and

$$B(E) = b^2 = 1 - A \qquad (2.32)$$

In any tunneling experiment, it is common to work with conductance derived from the differential conductance at zero temperature. This conductance is given by

$$\frac{dI}{dV} \propto T(E) . \qquad (2.33)$$

The differential conductance depends on the voltage V and on the height of potential barrier z.
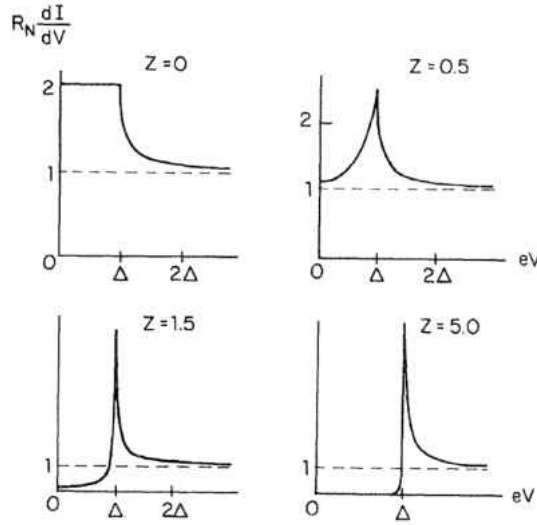
Figure 7: The result from reference [9] illustrates the curves for the differential tunneling conductance versus bias voltage for four different values of z (z = 0, 0.5, 1.5, and 5).

Finally, I note that the BTK theory is a mean field theory which describes the tunneling process between the normal metal and an s-wave superconductor. The conductance versus bias voltage V plot for four different potential barrier heights at zero

temperature is shown in Fig 7. In zero-barrier height ($z = 0$), the conductance within the superconducting gap is nearly doubled because most of the incident electrons are Andreev-reflected and the transmitted electron pairs across the interface carries double the amount of charge of the incident electrons. On the other hand, in the high-barrier limit, the result given by the BTK formalism is the same as the conductance plotted for z = 5. There is peak for higher value of the potential barrier height z which can exist because of existence of Andreev bound states near the edges [9].

2.4 Mid-gap bound states and super-current

The effect of Andreev bound state is to transport Cooper pairs and yields supercurrent. For a short Josephson junction, the DC Josephson Effect can be explained based on the current carried by the Andreev bound states. In a superconductor-normal metal-superconductor (SNS) junction with one-gap superconductors, there are two NS contacts. A more important description of Josephson tunneling current, based on the BdG model was introduced by Furusaki and Tsukada [10]. Here, the solutions of BdG equation are localized to the N side of the interface. These points are called Andreev bound states or mid-gap states. Their energy is in the middle of the superconducting gap and manifests themselves as a zero-bias peak in tunneling conductance into the corresponding edge. The existence of mid-gap states is related to the sign change of the pairing potential around the Fermi surface.

CHAPTER III

TWO-GAP SUPERCONDUCTORS

Two-band superconductivity has been a focus of much attention of superconductivity research community over the past many years. Most conventional superconductors have one-order parameter, reflecting one type of superconducting condensate and one energy gap. However some superconductors such as MgB_2 and iron-pnictides are known to have two superconducting gap structure. In 2001, superconductivity in MgB_2 transition temperature of about 40 Kelvin was discovered. Recently, in 2008, iron-based superconductors were discovered.

The Josephson junction with two-gap superconductors, including MgB_2 and iron pnictides, is a focus of much research in recent years due to its intriguing properties. Compared to one-gap superconductors such as mercury and niobium, the multi-gap superconductors such as MgB_2 and iron-pnictides have higher transition temperature (critical temperature) T_c and multiple channels for tunneling. One big interest about two-gap superconductivity is the presence of inter-band Josephson tunneling between the two superconducting electronic bands. This depends on the degree of sensitivity on scattering inside and between two superconducting condensates. The two-gap superconductors exist because of two electronic bands participate in superconductivity.

In this chapter, first, I discuss the experimental evidence for two-gap superconductivity in MgB_2 and iron pnictides. Then, I discuss the BCS theory for two-

gap superconductivity. Then, I explain two types of symmetry for the conventional superconducting order parameter.

3.1 MgB$_2$ and iron-based superconductors

Two most recently discovered two-gap superconductors are MgB$_2$ and iron compounds superconductors. In general, experimental data from specific heat, Andreev reflection spectroscopy, and microwave response measurement indicate the evidence of superconducting gap structures. Evidence of two-gap structures was found in MgB$_2$ and iron-based superconductors [11 - 18].

Fig. 8, the structure of MgB$_2$ is schematically illustrated. The crystal structure of MgB$_2$ is a honeycomb of boron layers and magnesium atoms are located between these layers. This material possesses a number of properties, which makes it promising for superconducting applications: it can be produced much easier than the high-T$_c$ cuprates, it is cheap, and it can be used as cheap substrates in high quality.

MgB$_2$ shows clear evidence of two-gap superconducting gaps of different size reside on different disconnected parts of its Fermi surface [30].
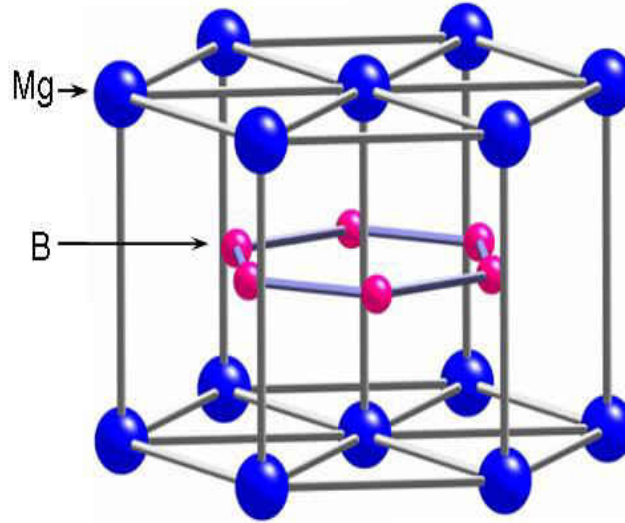
Figure 8: Crystal structure of MgB_2 [20] is illustrated schematically. Boron atoms from stacks of honeycomb layers and magnesium atoms are in between the boron layers at the center of the hexagons.

A theoretical investigation of the multi-band model for tunneling in MgB_2 junction shows that there is a possibility of observing either one or two gaps in the tunneling spectra of MgB_2, depending on the tunneling direction, barrier type and impurity concentration. Mazin and coworkers have suggested that the inter-band scattering between the σ and π band is exceptionally small because of the different symmetries of charge density of bands [21].

The experimental evidence on the order parameter is the key issue for understanding superconductivity in MgB_2. The experiments yielded observation of distinct gap features in tunneling spectra [22] by scanning tunneling microscopy and by point-contact techniques. However, the values reported by different experimental groups were at odds with each other, ranging from 1.5 meV to 7.5 meV. It was natural to assume that the low-gap data arose from the surface layer of the samples, which could have degraded the value of T_c. Tunneling spectroscopy is one of the powerful tools to measure the superconducting energy gap. A number of such measurements have been performed on

MgB$_2$ [22].   The Raman spectra of polycrystalline MgB$_2$ was measured from 25 to 1200 cm^{-1}, and found that two pair-breaking peaks appear in the spectra. These two peaks suggest the presence of two superconducting gaps[22].

The iron-pnictides are also well-known two-gap superconductors.   These superconductors were first discovered in 2008 and exhibit superconducting transition temperatures as high as about 55 K [23].   The family of iron-based superconductors are ReFeAsO, where Re is a Rare Earth metal, and AFe$_2$As$_2$, where A is an Alkaline Earth metal. The structures of two different iron-pnictide compounds are shown in Fig. 9.
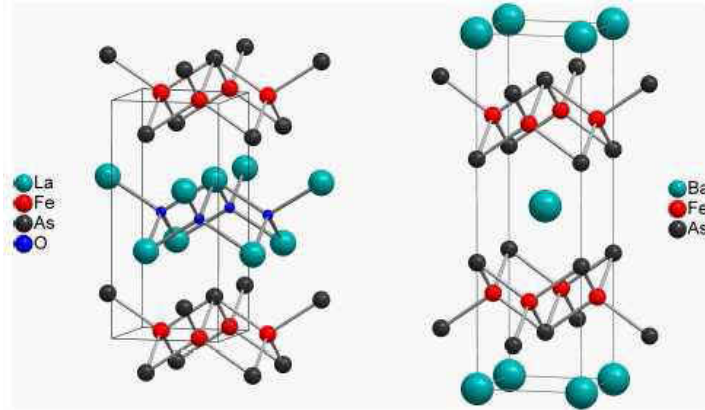
Figure 9:   The crystal structure of iron-based superconductor from reference [24] with the 1111, 122 of Arsenic is schematically illustrated.

Experimental studies show that the point-contact Andreev-reflection experiments performed on LaFeAsO$_{1-x}$F$_x$ (La-1111) polycrystalline samples with T$_c$ ~ 27 K and SmFeAsO$_{0.8}$F$_{0.2}$ (Sm-1111) polycrystalline sample with T$_c$ ~ 53 K gave differential conductance curves exhibiting two peaks at low bias and two additional structures (peaks) at higher bias voltages [23]. These results showed the clear evidence of two gaps in the superconducting state of ReFeAsO$_{1-x}$F$_x$ (Re = La, Sm): a small gap Δ_1 is smaller than the BCS value ($2\Delta_1/k_BT_c$ ~ 2.2 − 3.2) and a much larger than Δ_2 which gives a ratio

$2\Delta_2/k_BT_c \sim 6.5 - 9$. In Sm-1111, both gaps close at the same temperature. The temperature dependence of gap functions Δ_1 and Δ_2 show remarkable deviations from the BCS behavior at temperatures close to T_c. The results of the point-contact spectroscopy measurements in polycrystalline samples of two compounds $LaFeAsO_{1-x}F_x$ (La-1111) and $SmFeAsO_{1-x}F_x$ (Sm-1111) indicated the presence of two distinct sets of features, such as low-energy conductance peaks and higher energy peak. Surprisingly, the spectra look very similar to those measured in MgB_2. In any case both these energy scales are related to superconductivity and do not exist in the normal state. Scanning tunneling spectroscopic studies of $Ba(Fe_{1-x}Co_x)_2As_2$ (x = 0.06, 0.12) single crystals reveal direct evidence for predominantly two-gap superconductivity. These gaps decrease with increasing temperature and vanish above the superconducting transition temperature T_c. The two-gap nature and the slightly doping- and energy-dependent quasi-particle scattering interferences near the wave vectors $(\pm\pi,0)$ and $(0,\pm\pi)$ are consistent with sign-changing s-wave superconductivity [24].

3.2   BCS theory for two-gap superconductors

In this section, I present the BCS theory for two-gap superconductivity. The BCS theory is a Hartree-Fock approach [25] for describing superconductivity. In this theory, superconductivity arises as a result of electron pair formations when the effective attractive interaction between electrons dominates the repulsive Coulomb forces. The BCS model described the properties of simple superconductors. An interesting issue is to understand two-band superconductivity within the BCS theory. The two-gap superconductivity may lead to new interesting physics. In MgB_2, the existence of two

condensates leads to two pseudo-order parameters which I denote as Δ_s and Δ_d. The coexistence of two distinctive order parameters is useful for understanding the phase coherent effects in superconductors.

The BCS theory is useful in multi-component system. I now proceed by writing down the Hamiltonian for two-gap superconductor as

$$H_{TB} = \sum_k \left[\varepsilon_k^s c_{k,\sigma}^+ c_{k,\sigma} + \varepsilon_k^d d_{k,\sigma}^+ d_{k,\sigma} \right] + H_{pair} \tag{3.1}$$

where the Hamiltonian H_{pair} accounts for the pair interaction contribution

$$H_{pair} = -\sum_{k,k'} \left[V_{ss} c_{k\uparrow}^+ c_{-k\downarrow}^+ c_{-k'\downarrow} c_{k'\uparrow} + V_{dd} d_{k\uparrow}^+ d_{-k\downarrow}^+ d_{-k'\downarrow} d_{k'\uparrow} + V_{sd} \left(c_{k\uparrow}^+ c_{-k\downarrow}^+ d_{-k'\downarrow} d_{k'\uparrow} + h.c. \right) \right] \tag{3.2}$$

In Eqs. (3.1) and (3.2), the fermion operators c (c^+) and d (d^+) describe the annihilation (creation) of s-band and d-band electrons, respectively. The pairing Hamiltonian H_{pair} contains two-body interaction terms such as $c_{k\uparrow}^+ c_{-k\downarrow}^+ c_{-k'\downarrow} c_{k'\uparrow}$. In the mean-field theory, this two-body interaction term is approximated and is reduced to the effective one-body terms. This can be accomplished by using Wick's theorem. By using the Wick's theorem, I rewrite the first term in Eq. (3.2) as the sum of two contributions: kinetic energy term and pairing term. The kinetic energy term may be written as

$$\sum_{kk'} V_{ss} \left\{ \left\langle c_{-k\downarrow}^+ c_{-k'} \right\rangle c_{k\uparrow}^+ c_{k'\uparrow} + \left\langle c_{k\uparrow}^+ c_{k'\uparrow} \right\rangle c_{-k\downarrow} c_{-k'\downarrow} \right\} \tag{3.3}$$

while the pairing term may be expressed as

$$\sum_{kk'} V_{ss} \left\{ \left\langle c_{k\uparrow}^+ c_{-k\downarrow}^+ \right\rangle c_{-k'\downarrow} c_{k'\uparrow} + \left\langle c_{-k'\downarrow} c_{k'\uparrow} \right\rangle c_{k\uparrow}^+ c_{-k\downarrow}^+ \right\} \tag{3.4}$$

The kinetic energy term of Eq. (3.4) may be easily absorbed in ε_k^s, so I will ignore this term. By carrying out the similar calculation for the remaining three interaction terms in Eq. (3.2), I rewrite the pair Hamiltonian as

$$H_{pair} = -\sum_{k,k'} \Big[V_{ss} \Big(\big\langle c_{k\uparrow}^{+} c_{-k\downarrow}^{+} \big\rangle c_{-k'\downarrow} c_{k'\uparrow} + \big\langle c_{-k'\downarrow} c_{k'\uparrow} \big\rangle c_{k\uparrow}^{+} c_{-k\downarrow}^{+} \Big)$$

$$+ V_{dd} \Big(\big\langle d_{k\uparrow}^{+} d_{-k\downarrow}^{+} \big\rangle d_{-k'\downarrow} d_{k'\uparrow} + \big\langle d_{-k'\uparrow} d_{k'\downarrow} \big\rangle d_{k\uparrow}^{+} d_{-k\downarrow}^{+} \Big)$$

$$+ V_{sd} \Big(\big\langle c_{k\uparrow}^{+} c_{-k\downarrow}^{+} \big\rangle d_{-k'\downarrow} d_{k'\uparrow} + \big\langle d_{k\uparrow} d_{-k\downarrow} \big\rangle c_{k\uparrow}^{+} c_{-k\downarrow}^{+} + \big\langle c_{k\uparrow} c_{-k\downarrow} \big\rangle d_{-k'\downarrow}^{+} d_{k'\uparrow}^{+} + \big\langle d_{k\uparrow}^{+} d_{-k\downarrow}^{+} \big\rangle c_{k\uparrow} c_{-k\downarrow} \Big) \Big] \qquad (3.5)$$

Here, I define the gap parameter Δ for s and d-band condensate as

$$\Delta_s = -V_{ss} \big\langle c_{-k\downarrow} c_{k\uparrow} \big\rangle, \qquad \Delta_s^* = -V_{ss} \big\langle c_{k\uparrow}^{+} c_{-k\uparrow}^{+} \big\rangle \qquad (3.6)$$

and

$$\Delta_d = -V_{dd} \big\langle d_{-k\downarrow} d_{k\uparrow} \big\rangle, \qquad \Delta_d^* = -V_{dd} \big\langle d_{k\uparrow}^{+} d_{-k\uparrow}^{+} \big\rangle \qquad (3.7)$$

respectively. Similar to the BCS theory for one-gap superconductivity, the Bogoluibov transformation may be used to diagonalize the two-gap Hamiltonian. By following Suhl, Maththias, and Walker [25], I introduce the following transformation:

$$c_{k\downarrow} = \cos(\theta_k/2) e_{k\uparrow} + \sin(\theta_k/2) e_{-k\downarrow}^{*} \qquad (3.8)$$

$$d_{k\uparrow} = \cos(\varphi_k/2) f_{k\uparrow} + \sin(\phi_k/2) f_{-k\uparrow}^{*} \qquad (3.9)$$

$$c_{k\downarrow} = \cos(\theta_k/2) e_{k\downarrow} - \sin(\theta_k/2) e_{-k\uparrow}^{*} \qquad (3.10)$$

$$d_{k\downarrow} = \cos(\varphi_k/2) f_{k\downarrow} - \sin(\varphi_k/2) f_{-k\uparrow}^{*} \qquad (3.11)$$

Here, the parameters θ and φ can be obtained by substituting the fermion operators c, and d in the original Hamiltonian H_{TB}. The off-diagonal elements of the transformed matrix should be zero. I impose this condition by setting the coefficients to the term $e_k^{+} e_{-k}^{+}$, $e_k e_{-k}$, $f_k^{+} f_{-k}^{+}$ and $f_k f_{-k}$ to zero. By imposing these conditions, I obtain

$$\varepsilon_{ks} \sin\theta_k - [V_{sd}\Delta_d + V_{ss}\Delta_s]\cos\theta_k = 0 \qquad (3.12)$$

and

$$\varepsilon_{kd} \sin \varphi_k - [V_{dd}\Delta_d + V_{sd}\Delta_s] \cos \varphi_k = 0 \tag{3.13}$$

From Eqs. (3.13) and (3.14), I obtain the two-coupled gap equations for the s- and d-band condensate as

$$\Delta_d = \sum_k \sin \varphi_k [1 - 2f_d(E_{kd})] \tag{3.14}$$

and

$$\Delta_s = \frac{1}{2}\sum_k \sin \theta_k [1 - 2f_s(E_{ks})] \tag{3.15}$$

Here, these gap parameters are complex numbers. Also, $f_s(E_{ks})$ and $f_d(E_{kd})$ are the Fermi-Dirac distribution function for s- and d-band electrons. The number of quasi-particles in the s- and d-bands that are excited to energies E_{ks} and E_{kd} may be computed by using these distribution functions. These complex gap parameters may be written as $\Delta_s = |\Delta_s|e^{i\theta_s}$ and $\Delta_d = |\Delta_d|e^{i\theta_d}$ to account for the gap structure of two-gap superconductors. For simplicity, I will use the symbols Δ_1 and Δ_2 to represent Δ_s and Δ_d, respectively.

3.3 Pairing symmetry: S_{++} versus S_{+-}

Two-gap superconductor has two types of pairing symmetry. The relative phase of the two condensates reflects the pairing symmetry. The dynamics of the phase difference may be described by phase-lock of two condensates. If the two s-wave pseudo-order parameters have the same phase in the σ-band and π-band, then there will be 0-phase locking [26] between hole and electron band for condensates. The 0-phase-locked state represents the S_{++} pairing symmetry. Tanaka and coworkers indicated that the inter-band

interaction J is positive ($J > 0$) [27] for this pairing symmetry. If two bands have π-phase difference, the phase-locked state represents the S_{+-} pairing symmetry or known as the π-phase locked state. In this case, the inter-band interaction parameter J is negative ($J < 0$).

The multi-band superconductors such as MgB_2 and iron-pnictides have different a different phase-locked state as the ground state. The electronic pairing in MgB_2 is known as S_{++} symmetry. In MgB_2, there are two tunneling channels with the same phase. The contribution from each channel may add in a constructive way. Hence, the current-phase relation is similar to a single-band superconductor.

However, some experimental studies showed that iron-pnictide superconductors may have S_{+-} pairing symmetry. This conclusion for the iron-pnictides is still controversial since the result of some experimental measurements does not support the conclusion. In this type of symmetry, there are two tunneling channel. Note that, the contribution from each channel may be summed to yield the destructive as well as constructive interference effects in the tunneling currents. Hence, the existence of two gaps in the superconductors like MgB_2 or iron-pnictides may affect the properties of the interfaces.

3.4   Phase fluctuations of condensates

There are some fluctuation effects around the phase-lock state of two condensates. If the fluctuations are small, then there may be collective excitations in the junction reflecting small phase oscillations. In the multi-gap superconductors, these fluctuations are classified into two types. The out-of-phase fluctuations are known as the Josephson-Leggett (JL) mode, while the in-phase fluctuations are known as the Josephson-plasma

mode. The JL mode had been observed by Bloomberg and his coworkers [26]. These phase fluctuations are important in long Josephson junctions (LJJ). Since the total energy of the two-gap superconductors depends on the relative phase of the condensates and the relative density of electrons, the phase dynamics of LJJ are affected by JL mode. The fluctuations about the phase-locked state may not necessarily remain small. They may become large. If the amplitude of fluctuations in the relative phase of the two condensates becomes large and the non-linear phase oscillations become stabilized, a 2π-phase texture known as i-soliton may appear. Excitation of i-soliton as shown in Fig. 11 can change the amplitude of the critical current density [27].
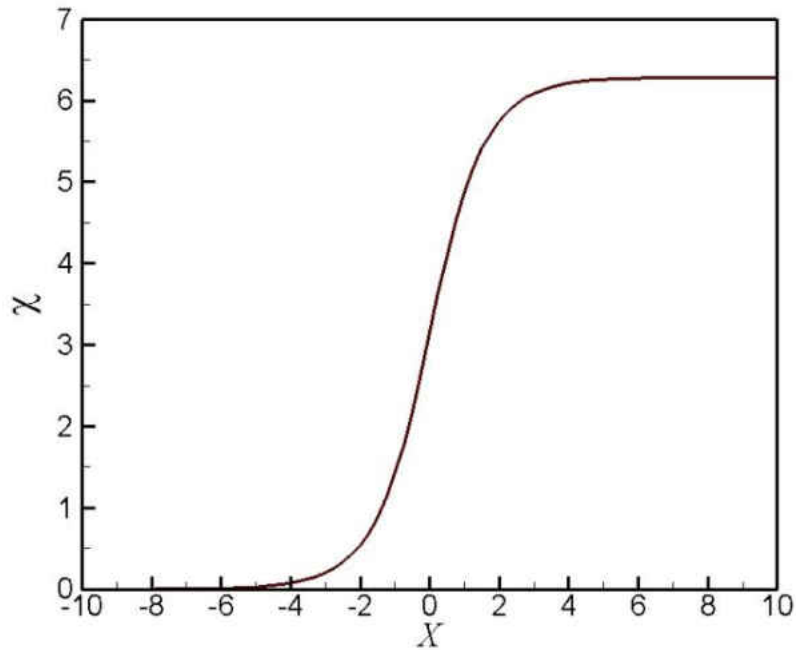
Figure 10: Relative phase difference χ of two order parameter is plotted as a function of position x in order to illustrate the single-kink solution. There is a phase change at $\chi = \pi$.

There is experimental evidence for i-soliton in two-gap superconductors. The magnetic response of a superconducting ring experiment with two pseudo-order parameters indicates that a stable i-soliton shaped phase difference χ between the two condensates is attainable [28]. This result indicates that the phase fluctuations can produce a 2π-phase texture [29]. The effects of phase fluctuations can appear as either additional resonance in the AC Josephson effect or a static 2π-kink in the phase difference. If the 2π-phase exists in each S layer, then this i-soliton may change the phase dynamics. In recent work of Kim, Ghimire, and Tsai [33], they showed that the formation of the 2π-phase kink in LJJ involving two-gap superconductors can affect the Josephson critical current density.

CHAPTER IV

ANDREEV BOUND STATES IN TWO-GAP SUPERCONDUCTOR JUNCTIONS

For two-gap superconductors, the presence of two condensates is important for determining the superconducting property. In this chapter, the Andreev reflection at the NS interface involving a two-gap superconductor is discussed. I follow the work of Golubov and coworkers and apply the approach used in the BTK theory to the superconductor junction with the S_{++} and S_{+-} pairing symmetry [32]. Then I will explain the appearance of mid-gap bound states at the surface of the normal metal-superconductor interface by using the Bloch waves.

4.1 Evidence of surface states

Existence of mid-gap states at the surface of two-gap superconductor junction had been an intriguing subject in recent years. There are many theoretical papers discussing the role of the mid-gap surface states in an SNS junction. Recent studies on a tunnel junction involving iron-pnictide superconductors showed that the mid-gap states may exist in the normal metal-superconductor 1-superconductor 2 (N-S_1-S_2) junction [31]. Feng and Ng showed that the quasi-particle can tunnel through the junction involving a

multi-band superconductor with S_{+-} pairing symmetry. In their calculation, Feng and Ng used plane waves as wave functions.

4.2 Bloch waves

All of the earlier studies used the plane waves to construct a wave function for both normal metal and superconductor for calculation of the bound state energy. As noted by Golubov and coworkers, the main pitfall of using the plane wave approach is that two different plane waves cannot propagate in the same direction with the same energy. To overcome this difficulty, Golubov and coworkers used Bloch waves to determine bound states in multiband superconductors [32]. According to Bloch's theorem, the eigen function of a system can be written as the product of a plane wave envelope function and a periodic Bloch function $u_{nk}(r)$. The Bloch wave function is given by

$$\psi_{nk}(r) = \sum_G u_{nk}(r) e^{i(k+G) \cdot r} \tag{4.1}$$

By using Bloch waves, I construct the wave function for both sides of the normal metal junction involving one-band metal on the left side and two-band metal on the right side. The wave function in the one-band normal metal side (i.e., left side or for $x < 0$) of the junction is given by

$$\Psi_N(x) = \psi_k(x) + b\psi_{-k}(x) \tag{4.2}$$

Here, the first term of Eq. (4.2) is the incident Bloch wave and the second term is the reflected one. For the two-band normal metal side (i.e., right side or for $x > 0$), the wave function is

$$\Psi_N(x) = c[\phi_p(x) + \alpha_0 \phi_q(x)] \tag{4.3}$$

where p and q denotes the Fermi vector for the s-band and d-band, respectively. Here, ϕ
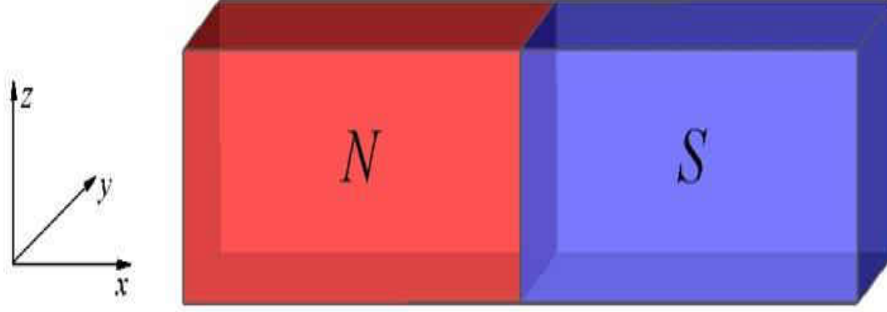
Figure 11: The Normal metal-Superconductor (NS) contact junction is schematically illustrated. The interface is located at x=0.

denotes the Bloch wave function similar to Eq. (4.1), and α_0 is the mixing coefficient which represents the ratio of probability for an electron flowing from left side to the right side. In the following sections, I will explain the details of the calculation of bound state energy for the NS junction involving a two-gap superconductor, similar to that done by Golubov and coworkers for a ballistic Andreev contact.

4.3 Bound states in SN interface

Following the work of Golubov and coworkers, I examine the NS junction. Here, all scattering is characterized by the phenomenological parameter z. The scattering potential is given by

$$V_{Barrier} = \frac{z\hbar^2 p_F}{m_e} \delta(x) \tag{4.4}$$

where p_F is the Fermi momentum in the superconductor. This potential barrier located at $x = 0$, as shown Fig. 11. Note that, that the two-gap superconductor has unequal s-wave symmetry gaps. The total wave function is given by

$$\Psi(x) = \Psi_N(x)\Theta(-x) + \Psi_S(x)\Theta(x) \tag{4.5}$$

where $\Theta(x)$ is the step-function. The wave function $\Psi_N(x)$ for the one-band normal metal is given by

$$\Psi_N(x) = \psi_k(x)\begin{pmatrix}1\\0\end{pmatrix} + a\psi_k(x)\begin{pmatrix}0\\1\end{pmatrix} + b\psi_{-k}(x)\begin{pmatrix}1\\0\end{pmatrix} \tag{4.6}$$

The wave function $\Psi_S(x)$ for the two-band superconductor is given by

$$\Psi_S(x) = c\left[\phi_p\begin{pmatrix}u_1\\v_1 e^{-i\theta_1}\end{pmatrix} + \alpha_0\phi_q\begin{pmatrix}u_2\\v_2 e^{-i\theta_2}\end{pmatrix}\right] + d\left[\phi_{-p}\begin{pmatrix}v_1\\u_1 e^{-i\theta_1}\end{pmatrix} + \alpha_0\phi_{-q}\begin{pmatrix}v_2\\u_2 e^{-i\theta_2}\end{pmatrix}\right] \tag{4.7}$$

The wave functions for the NS junction have two components. The first component indicates the wave function for the electron, and the second component represents the wave function for the hole. Here, the parameter α_0 accounts for wave function mixing, similar to that in Eq. (4.3). The coherence factor for a particle $u_{1,2}$ and for a hole $v_{1,2}$ are given, respectively, as

$$u_{1,2}^2 = \frac{1}{2}\left(1 + \frac{\sqrt{E^2 - \Delta_{1,2}^2}}{E}\right) \tag{4.9}$$

and

$$v_{1,2}^2 = \frac{1}{2}\left(1 - \frac{\sqrt{E^2 - \Delta_{1,2}^2}}{E}\right) \tag{4.10}$$

where $\Delta_{1,2}$ represents the magnitude of the superconductor order parameter. In the case of the S_{+-} pairing symmetry, a superconductor with unequal gaps of opposite sign has the phase difference of $\theta_1 - \theta_2 = \pi$. However, for the standard S_{++} pairing symmetry, a

superconductor with unequal gaps of the same sign has $\theta_1 = \theta_2$. The amplitudes a and b in the wave function (4.6) describe Andreev and normal reflection, respectively. The amplitudes c and d describe transmission without branch crossing and with branch crossing, respectively. To solve this one-dimensional quantum mechanical scattering problem and obtain bound state energy, I impose two boundary conditions: the wave function must be i) continuous and ii) smooth. The continuity of wave functions at the interface (i.e., x=0) yields

$$\Psi_N(0) = \Psi_S(0) = \Psi(0) \tag{4.10}$$

By applying the boundary condition of Eq. (4.10), the wave function can be divided into two equations corresponding to electrons and holes. These two equations may be written as

$$a\left[v_1 e^{-i\theta_1} + \alpha_0 \frac{\phi_q(0)}{\phi_p(0)} v_2 e^{-i\theta_2} \right] + b \frac{\phi_{-p}(0)}{\phi_p(0)} \left[u_1 e^{-i\theta_1} + \alpha_0 \frac{\phi_{-q}(0)}{\phi_{-p}(0)} u_2 e^{-i\theta_2} \right] = \alpha \frac{\psi_k(0)}{\phi_p(0)} \tag{4.11}$$

and

$$a\left[u_1 + \alpha_0 \frac{\phi_q(0)}{\phi_p(0)} u_2 \right] + b \frac{\phi_{-p}(0)}{\phi_p(0)} \left[v_1 + \alpha_0 \frac{\phi_{-q}(0)}{\phi_{-p}(0)} v_2 \right] = \frac{\psi_k(0)}{\phi_p(0)} + \beta \frac{\psi_{-k}(0)}{\phi_p(0)} \tag{4.12}$$

Now, I impose the second boundary condition of smoothness which is given by

$$\frac{\hbar^2}{2m} \frac{d\Psi_S(x)}{dx}\bigg|_{x=0^+} - \frac{\hbar^2}{2m} \frac{d\Psi_N(x)}{dx}\bigg|_{x=0^-} = \Lambda\Psi(0) \tag{4.13}$$

By applying the condition of Eq. (4.13), I obtain two equations, again, corresponding to electrons and holes. These two equations are written as

$$aZ[u_1 + \overline{\alpha_0}u_2] - b\frac{\phi_{-p}(0)}{\phi_p(0)} Z^*[v_1 + \alpha_0 v_2] + \beta \frac{\psi_{-k}(0)}{\phi_p(0)} Z = -\frac{\psi_k(0)}{\phi_p(0)} Z^* \tag{4.14}$$

and

$$aZ[v_1 e^{-i\theta_1} + \overline{\alpha_0} v_2 e^{-i\theta_2}] - b\frac{\phi_{-p}(0)}{\phi_p(0)} Z^*[u_1 e^{-i\theta_1} + \alpha_0 u_2 e^{-i\theta_2}] = \alpha \frac{\psi_k(0)}{\phi_p(0)} Z^* \qquad (4.15)$$

where the complex parameter $Z = 1 + i\,z$ to simplify the problem. Here, the parameter z indicates the height of potential barrier. The parameter z can be written as

$$z = \frac{\Lambda}{\hbar v_F} \qquad (4.16)$$

where Λ is the strength of the potential barrier and v_F is the Fermi velocity. I note that the interface velocity $\overline{v}_k$, which is defined as

$$\overline{v}_k = -\frac{i\hbar}{m} \frac{1}{\psi_k(x)} \frac{d\psi_k(x)}{d(x)}\bigg|_{x=0} \qquad (4.17)$$

has the same property as Fermi velocity v_F. This velocity is real and has the same property as the group velocity. For simplicity, I introduce the parameter η which is defined as

$$\eta = \alpha_o \frac{\phi_{\pm q}(0)}{\phi_{\pm p}(0)} \qquad (4.18)$$

at the interface ($x = 0$). Now, I need to solve the four coupled equations (4.11), (4.12), (4.14), and (4.15) to find the coefficients a, b, c and d. These coefficients can be obtained solving

$$M_{SN} Y_{SN} = 0$$

where the matrix M_{SN} is given by

$$M_{SN} = \begin{pmatrix} u_1 + \eta u_2 & v_1 + \eta v_2 & 0 & -1 \\ v_1 e^{-i\theta_1} + \eta v_2 e^{-i\theta_2} & u_1 e^{-i\theta_1} + \eta u_2 e^{-i\theta_2} & -1 & 0 \\ Z[u_1 + \eta u_2] & -Z^*[v_1 + \eta_0 v_2] & 0 & Z \\ Z[v_1 e^{-i\theta_1} + \eta v_2 e^{-i\theta_2}] & -Z^*[u_1 e^{-i\theta_1} + \eta u_2 e^{-i\theta_2}] & -Z^* & 0 \end{pmatrix} \qquad (4.19)$$

and the column matrix Y_{SN} is given by

$$Y_{SN}^T = \left(a \quad b\frac{\phi_{-p}(0)}{\phi_p(0)} \quad c\frac{\phi_{-p}(0)}{\phi_p(0)} \quad d \right) \qquad (4.20)$$

To find the bound state energy, I need to solve the secular equation. So, I set the determinant of matrix M_{SN} to zero

$$\det M_{SN} = 0 \qquad (4.21)$$

It is straightforward to see that Eq. (4.21) may be written as

$$e^{-i\theta_1}[u_1 U(1+z^2) - v_1 Vz^2] + \eta e^{-i\theta_1}[u_2 U(1+z^2) - v_2 Vz^2] = 0 \qquad (4.22)$$

where $U = (u_1 + \bar{\alpha}_0 u_2)$ and $V = (v_1 + \bar{\alpha}_0 v_2)$. I note that Eq. (4.22) will serve as the central equation for computing the bound state energies.

Now, I find the solution of Eq. (4.22) for the two special cases: i) the transparent ($z = 0$) case and ii) the insulating (large Z) case. First, for the z=0 case which corresponds to the transparent interface, Eq. (4.22) simplifies to

$$(u_1 e^{-i\theta_1} + \eta u_2 e^{-i\theta_2})(u_1 + \eta u_2) = 0 \qquad (4.23)$$

I simplify Eq. (4.23) further by considering the S_{++} pairing symmetry by setting the phase of the condensates as $\theta_1 = \theta_2 = 0$ (i.e., $\chi = \theta_s - \theta_d = 0$). For this case, the bound state energy may be found by solving

$$\left(1 + \frac{\sqrt{E^2 - \Delta_1^2}}{E} \right)^{1/2} + \eta\left(1 + \frac{\sqrt{E^2 - \Delta_2^2}}{E} \right)^{1/2} = 0 \qquad (4.24)$$

However, there is no solution to Eq. (4.24), suggesting that there is no bound state energy solution. Next, I look for the bound state energy for the S_{+-} pairing symmetry by setting

the phase of the condensates as $\theta_1 = \pi$ and $\theta_2 = 0$. For this case, Eq. (4.23) may simplify to

$$1 + \frac{\sqrt{E^2 - \Delta_1^2}}{E} = \eta^2 \left(1 + \frac{\sqrt{E^2 - \Delta_2^2}}{E} \right) \tag{4.25}$$

I solve Eq. (4.25) for the bound state energy and obtain

$$E_B = \frac{\Delta_s^2 - \eta^4 \Delta_d^2}{2\eta \sqrt{1 - \eta^2} \sqrt{\Delta_s^2 - \eta^2 \Delta_d^2}} \tag{4.27}$$

The bound state energy of Eq. (4.27) indicates that, when the phase differences of s and d band condensate is π (i.e., $\chi = \theta_s - \theta_d = \pi$), the zero energy mid-gap state appears for $\Delta_s = \eta^2 \Delta_d$. Now, I compute the bound state energy for weakly transparent interface (i.e., z $\gg 1$). In this case, the secular equation of (4.22) simplifies to

$$e^{-i\theta_1}[u_1(u_1 + \eta u_2) - v_1(v_1 + \eta v_2)] + e^{-i\theta_1}\eta[u_2(u_1 + \eta u_2) - v_2(v_1 + \eta v_2)] = 0 \tag{4.28}$$

I consider the S_{++} pairing symmetry case by setting the phase as $\chi = \theta_s - \theta_d = 0$. For this case, Eq. (4.28) can be written as

$$(u_1 + \eta u_2)^2 - (v_1 + \eta v_2)^2 = 0 \tag{4.29}$$

Equation (4.29) can be expanded and rewritten as

$$(u_1^2 - v_1^2) + \eta^2(u_2^2 - v_2^2) + 2\eta(u_1 u_2 - v_1 v_2) = 0 \tag{4.30}$$

Using the expression for the coherence factor $u_{1,2}$ and $v_{1,2}$ for particles and holes, respectively, I simplify Eq. (4.30) further and write

$$E^2(1 + \eta^2)^2 = \Delta_1^2 + \eta^4 \Delta_2^2 - 2\eta^2 \Delta_1 \Delta_2 \tag{4.32}$$

From Eq. (4.32), it is straightforward to see that the bound state energy for the S_{++}-symmetry superconductor is given by

$$E_B = \pm \frac{\Delta_1 - \eta^2 \Delta_2}{1 + \eta^2} \tag{4.33}$$

For S_{+-} pairing symmetry, I set the phases to $\chi = \theta_s - \theta_d = \pi$ and look for the bound state energy for the low transparency case (i.e., $z \gg 1$). In this case, the secular equation (4.28) simplifies to

$$(u_1^2 - v_1^2) - \eta^2 (u_2^2 - v_2^2) = 0 \tag{4.34}$$

Once again, I substitute the expression for the coherence factors $u_{1,2}$ and $v_{1,2}$ into Eq. (4.34) and obtain

$$\frac{\sqrt{E_B^2 - \Delta_1^2}}{E_B} = \eta^2 \frac{\sqrt{E_B^2 - \Delta_2^2}}{E_B} \tag{4.35}$$

The bound state energy obtained from Eq. (4.35) is

$$E_B = \pm \sqrt{\frac{\Delta_1^2 - \eta^4 \Delta_2^2}{1 - \eta^4}} \tag{4.36}$$

This bound state energy at the interface yields the peaks in the differential conductance for SN junction. Here, if $\Delta_1 = \Delta_2 = \Delta$, Eq. (4.33) yields the trivial solution of $E_B = \Delta$, indicating that there is no mid gap states. For the $\eta = 0$ case, the similar solution of $E_B = \Delta_1$ is obtained. For $0 \ll \eta \ll \Delta_1 / \Delta_2$, however, the $E_B = 0$ bound state exists if $\eta = \Delta_1 / \Delta_2$.

CHAPTER V

MID-GAP STATES IN SIS JUNCTION

In recent years, there has been a growing interest in superconducting-normal metal-superconducting (SNS) tunnel junctions. In this chapter, I investigate the mid-gap states in the superconductor-insulator-superconductor (SIS) break junction as shown in Fig. 12. In this type of the junction, the insulator layer is very thin. I examine the S_{++} and S_{+-} pairing symmetry with unequal s-wave gaps in two bands. Also, I discuss the effects of interference between the electron wave functions from the two electronic bands. The two-gap superconductors in the junction are represented by two pseudo-order parameters $\Delta_1 = \Delta_1 e^{i\theta_1}$ and $\Delta_2 = \Delta_2 e^{i\theta_2}$. In the two-gap superconductors, there are two tunneling channels. Theses tunneling channels indicate two different kinds of phase differences, suggesting that there are two types of Josephson effects. These are the usual Josephson effects between two adjacent superconductor layers as well as the inter-band Josephson effects between two condensates. The inter-band Josephson effects is needed to account for tunneling of quasi-particles between the two electronic bands in the same S layer. The inter-band Josephson effects drive the dynamics of the phase difference between the two condensates.
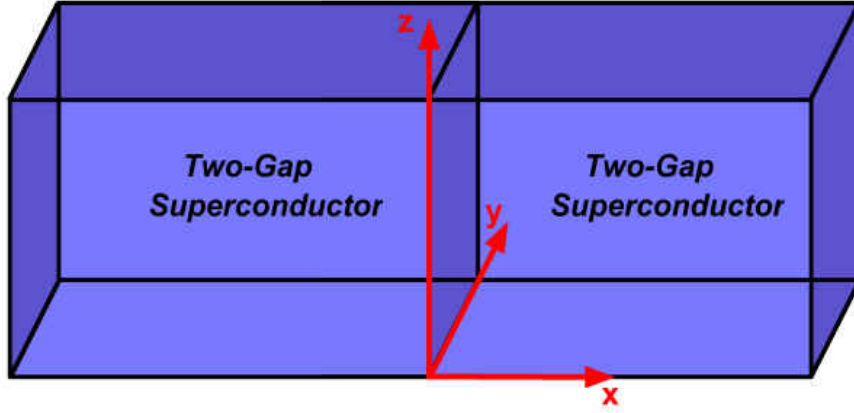
Figure 12: A schematic diagram of two-gap Josephson break junction (SIS) is illustrated. Insulator is a thin layer which is the yz surface located at x=0 between the two superconductors.

5.1 Wave function for the superconducting state

I investigate the in-gap state of the break junction involving a two-gap superconductor. I start the calculation by writing the wave function for each side of the junction. Assuming that the junction barrier is located at x = 0, the wave function for the two superconductor side of the junction may be written as

$$\Psi(x) = \Psi_{SL}\Theta(-x) + \Psi_{SR}\Theta(x) \tag{5.1}$$

where $\Theta(x)$ is the step function. Here, L and R refer to left and right side superconductor, respectively. In particular, the wave functions for the superconductor on the left side of the barrier potential is given by

$$\Psi_{SL}(x) = a\left[\phi_{-p}\begin{pmatrix} u_1 \\ v_1 e^{-i\theta_1^L} \end{pmatrix} + \alpha_0\phi_{-q}\begin{pmatrix} u_2 \\ v_2 e^{-i\theta_2^L} \end{pmatrix}\right] + b\left[\phi_p\begin{pmatrix} v_1 \\ u_1 e^{-i\theta_1^L} \end{pmatrix} + \alpha_0\phi_q\begin{pmatrix} v_2 \\ u_2 e^{-i\theta_2^L} \end{pmatrix}\right] \tag{5.2}$$

Note that p and q denote the momentum of particle in s-band and d-band, respectively. Here, $\phi_{\pm p}$ (x) and $\phi_{\pm q}$ (x) are Bloch wave functions. Also, the wave function for the superconductor on the right side of the potential barrier is given by

44

$$\Psi_{SR}(x) = c\left[\phi_p\begin{pmatrix} u_1 \\ v_1 e^{-i\theta_1^R} \end{pmatrix} + \alpha_0\phi_{-q}\begin{pmatrix} u_2 \\ v_2 e^{-i\theta_2^R} \end{pmatrix}\right] + d\left[\phi_{-p}\begin{pmatrix} v_1 \\ u_1 e^{-i\theta_1^R} \end{pmatrix} + \alpha_0\phi_{-q}\begin{pmatrix} v_2 \\ u_2 e^{-i\theta_2^R} \end{pmatrix}\right] \quad (5.3)$$

Here, α_0 is the mixing parameter. The coefficients a and b in Eq. (5.2) describe Andreev and normal reflection at the interface, respectively. The coefficients c and d indicate transmission with no branch crossing and with branch crossing, respectively [32]. I note that u_i and v_i are the usual Bogoliubov coefficients for the particle and hole representing the coherence factors, respectively.

Since I am treating this problem as a quantum mechanical potential scattering problem, the wave function must satisfy the boundary conditions at the interface. As discussed in Chapter 4, there are two boundary conditions: the wave function must be i) continuous and ii) smooth. The first condition requires that the superconductor wave function on the both sides of the potential barrier is equal to each other at the interface (i.e., continuity condition). So, the first boundary condition at the interface (x = 0) is given by

$$\Psi_{SL}(0) = \Psi_{SR}(0) = \Psi(0) \quad (5.4)$$

Since the wave function for each superconductor has the particle and hole components, the boundary condition of Eq. (5.4) yields the following two equations:

$$a[u_1 + \alpha_0 \frac{\phi_q(0)}{\phi_p(0)} u_2] + b\frac{\phi_{-p}(0)}{\phi_p(0)}[v_1 + \alpha_0 \frac{\phi_{-q}(0)}{\phi_{-p}(0)} v_2] =$$

$$c\frac{\phi_{-p}(0)}{\phi_p(0)}[u_1 + \alpha_0 \frac{\phi_{-q}(0)}{\phi_{-p}(0)} u_2] + d[v_1 + \alpha_0 \frac{\phi_q(0)}{\phi_p(0)} v_2] \quad (5.5)$$

and

$$a[v_1 e^{-i\theta_1^R} + \alpha_0 \frac{\phi_q(0)}{\phi_p(0)} v_2 e^{-i\theta_2^R}] + b\frac{\phi_{-p}(0)}{\phi_p(0)}[u_1 e^{-i\theta_1^R} + \alpha_0 \frac{\phi_{-q}(0)}{\phi_{-p}(0)} u_2 e^{-i\theta_2^R}] =$$

$$c \frac{\phi_{-p}(0)}{\phi_p(0)} \left[v_1 e^{-i\theta_1^L} + \alpha_0 \frac{\phi_{-q}(0)}{\phi_{-p}(0)} v_2 e^{-i\theta_2^L} \right] + d[u_1 e^{-i\theta_1^L} + \alpha_0 \frac{\phi_q(0)}{\phi_p(0)} u_2 e^{-i\theta_2^L}] \qquad (5.6)$$

Now by applying the second boundary condition, the wave function on each side of the barrier must satisfy

$$\frac{\hbar^2}{2m} \frac{d\Psi_{SR}}{dx}\bigg|_{x=0^+} - \frac{\hbar^2}{2m} \frac{d\Psi_{SL}}{dx}\bigg|_{x=0^-} = H_0 \Psi(0) \qquad (5.7)$$

I note that Eq. (5.7) may be derived easily from the Schrödinger equation for the wave function $\Psi(x)$. Inserting the wave functions into Eq. (5.7), the following two equations are obtained

$$\frac{\hbar^2}{2m} \left\{ a\left[\frac{d\phi_p(x)}{dx} u_1 + \alpha_0 \frac{d\phi_q(x)}{dx} u_2 \right] + b\left[\frac{d\phi_{-p}(x)}{dx} v_1 + \alpha_0 \frac{d\phi_{-q}(x)}{dx} v_2 \right] \right\}_{x=0^+}$$

$$- \frac{\hbar^2}{2m} \left\{ c\left[\frac{d\phi_{-p}(X)}{dX} u_1 + \alpha_0 \frac{d\phi_{-q}(X)}{dX} u_2 \right] + d[\frac{d\phi_p(X)}{dX} v_1 + \alpha_0 \frac{d\phi_q(X)}{dX} v_2] \right\}_{x=0^-}$$

$$= \frac{\Lambda}{2} \{a[\phi_p(0)u_1 + \alpha_0\phi_q(0)u_2] + b[\phi_{-p}(0)v_1 + \alpha_0\phi_{-q}(0)v_2]$$

$$+ c[\phi_{-p}(0)u_1 + \alpha_0\phi_{-q}(0)u_2] + d[\phi_p(0)v_1 + \alpha_0\phi_q(0)v_2]\} \qquad (5.8)$$

and

$$\frac{\hbar^2}{2m} \left\{ a\left[\frac{1}{\phi_p} \frac{d\phi_p}{dx} u_1 + \alpha_0 \frac{\phi_q}{\phi_p} \frac{1}{\phi_q} \frac{d\phi_q}{dx} u_2 \right] + b\left[\frac{d\phi_{-p}}{dx} v_1 e^{-i\theta_1^R} + \alpha_0 \frac{d\phi_{-q}}{dx} v_2 e^{-i\theta_2^R} \right] \right\}_{x=0^+}$$

$$- \frac{\hbar^2}{2m} \left\{ c\left[\frac{d\phi_{-p}}{dx} u_1 e^{-i\theta_1^L} + \alpha_0 \frac{d\phi_{-q}}{dx} u_2 e^{-i\theta_2^L} \right] + d\left[\frac{d\phi_p}{dx} v_1 e^{-i\theta_1^L} + \alpha_0 \frac{d\phi_q}{dx} v_2 e^{-i\theta_2^L} \right] \right\}_{x=0^+}$$

$$= \frac{\Lambda}{2} \{a[\phi_p(0)u_1 e^{-i\theta_1^R} + \alpha_0\phi_q(0)u_2 e^{-i\theta_2^R}] + b[\phi_{-p}(0)v_1 e^{-i\theta_1^R} + \alpha_0\phi_{-q}(0)v_2 e^{-i\theta_2^R}]$$

$$+ c[\phi_{-p}(0)u_1 e^{-i\theta_1^L} + \alpha_0\phi_{-q}(0)u_2 e^{-i\theta_2^L}] + d[\phi_p(0)v_1 e^{-i\theta_1^L} + \alpha_0\phi_q(0)v_2 e^{-i\theta_2^L}]\} \qquad (5.9)$$

As shown above, after applying the boundary conditions at the interface, four equations are obtained. These four coupled equations from the boundary conditions may be expressed in a simpler form by writing them as a matrix equation $M_{SIS}Y_{SIS} = 0$, the secular equation, where the 4x4 matrix M_{SIS} is given by

$$M_{SIS} = \begin{bmatrix} \overline{U}_0 & \overline{V}_0 & -\overline{U}_0 & -\overline{V}_0 \\ \overline{V}_{\theta_1} & \overline{U}_{\theta_1} & -\overline{V}_{\theta_2} & -\overline{U}_{\theta_2} \\ Z\overline{U}_0 & -Z^*\overline{V}_0 & Z\overline{U}_0 & -Z^*\overline{V}_0 \\ Z\overline{V}_{\theta_1} & -Z^*\overline{U}_{\theta_1} & Z\overline{V}_{\theta_2} & -Z^*\overline{U}_{\theta_2} \end{bmatrix} \tag{5.10}$$

and the column matrix Y_{SIS} is given by

$$Y_{SIS}^T = \begin{pmatrix} a & b\dfrac{\phi_{-p}(0)}{\phi_p(0)} & c\dfrac{\phi_{-p}(0)}{\phi_p(0)} & d \end{pmatrix} \tag{5.11}$$

Here, $Z = 1 + iz$ and the factors in the elements of M_{SIS} are defined as

$$\overline{V}_0 = v_1 + \eta v_2 \tag{5.12}$$

$$\overline{U}_0 = u_1 + \eta u_2 \tag{5.13}$$

$$\overline{V}_{\theta_1} = v_1 e^{-i\theta_1^R} + \eta v_2 e^{-i\theta_2^R} \tag{5.14}$$

$$\overline{U}_{\theta_1} = u_1 e^{-i\theta_1^R} + \eta u_2 e^{-i\theta_2^R} \tag{5.15}$$

$$\overline{V}_{\theta_1} = v_1 e^{-i\theta_1^L} + \eta v_2 e^{-i\theta_2^L} \tag{5.16}$$

and

$$\overline{U}_{\theta_2} = u_1 e^{-i\theta_1^R} + \eta u_2 e^{-i\theta_2^R} \tag{5.17}$$

Here, η is defined in Eq. (4.18) as

$$\eta = \alpha_o \frac{\phi_{\pm q}(0)}{\phi_{\pm p}(0)}$$

47

The phase differences between the two condensates in the left and right superconductor, respectively, are defined as

$$\theta_2^L - \theta_1^L = \chi^L \quad \text{and} \quad \theta_2^R - \theta_1^R = \chi^R \tag{5.18}$$

Next, I will solve the secular equation by

$$\det M_{SIS} = 0 \tag{5.19}$$

Equation (5.19) may be written as a fourth order polynomial equation in η

$$0 = \sum_{i=0}^{4} a_i \eta^i \tag{5.20}$$

where the coefficients a_i may be defined as the following:

$$a_0 = u_1^2 v_1^2 (e^{i\varphi^{ss}} + e^{-i\varphi^{ss}}) + 2u_1^2 v_1^2 z - (u_1^4 + v_1^4)(1 + z^2) \tag{5.21}$$

$$a_1 = (u_1^2 v_1 v_2 + v_1^2 u_1 u_2)[e^{i\varphi^{ss}} + e^{-i\varphi^{ss}} + e^{i(\varphi^{ss} - \chi^L)} + e^{-i(\varphi^{ss} - \chi^L)}]$$

$$+ [(u_1^2 v_1 v_2 + v_1^2 u_1 u_2) z^2 - (u_1^2 u_1 u_2 + v_1^2 v_1 v_2)(1 + z^2)](2 + e^{-i\chi^R} + e^{-i\chi^L}) \tag{5.22}$$

$$a_2 = u_1 u_2 v_1 v_2 [e^{i\varphi^{ss}} + e^{-i\varphi^{ss}} + 2e^{i(\varphi^{ss} - \chi^L)} + 2e^{-i(\varphi^{ss} + \chi^R)} + e^{i(\varphi^{ss} - 2\chi^L)} + e^{-i(\varphi^{ss} - 2\chi^R)}]$$

$$+ [2u_1 u_2 v_1 v_2 z^2 - (u_1^2 u_2^2 + v_1^2 v_2^2)(1 + z^2)][1 + e^{-i\chi^R} + e^{-\chi^L} + e^{-i(\chi^L + \chi^R)}]$$

$$+ (u_1^2 v_1^2 + u_2^2 v_1^2)[e^{i(\varphi^{ss} - \chi^L)} + e^{-i(\varphi^{ss} + \chi^R)}]$$

$$+ [(u_1^2 v_2^2 + u_2^2 v_1^2) z^2 - (u_1^2 u_2^2 + v_1^2 v_2^2)(1 + z^2)(e^{-i\chi^R} + e^{-i\chi^L}) \tag{5.23}$$

$$a_3 = (u_2^2 v_1 v_2 + v_2^2 u_1 u_2)[e^{i(\varphi^{ss} - \chi^L)} + e^{-i(\varphi^{ss} + \chi^R)} + e^{i(\varphi^{ss} - 2\chi^L)} + e^{-i(\varphi^{ss} + 2\chi^R)}]$$

$$+ (u_2^2 v_1 v_2 + v_2^2 u_1 u_2)[e^{i(\varphi^{ss} - \chi^L)} + e^{-i(\varphi^{ss} + \chi^R)} + e^{i(\varphi^{ss} - 2\chi^L)} + e^{-i(\varphi^{ss} + 2\chi^R)}]$$

(5.24)

and

$$a_4 = u_2^2 v_2^2 [e^{i(\varphi^{ss} - 2\chi^L)} + e^{-i(\varphi^{ss} + 2\chi^R)}] + [2u_2^2 v_2^2 z - (u_2^4 + v_2^4)(1 + z^2)]e^{-i(\chi^R + \chi^L)} \tag{5.25}$$

Here, $\varphi^{ss} = \theta_1{}^L - \theta_1{}^R$ is the phase difference between the s-band condensates in two adjacent superconductor islands. In order to find the mid-gap states, I need to solve Eq. (5.20) by using the phase difference between the two condensates within each superconductor that minimizes the free energy. Recent work of Kim indicates that the Ginzburg-Landau free energy for the two-gap superconductor Josephson junction is minimized when $\chi^L = \chi_0$ and $\chi^R = -\chi_0$. This substitution for both χ^L and χ^R simplifies Eq. (5.20) to

$$0 = \sum_{i=0}^{4} b_i \eta^i \qquad (5.26)$$

where the coefficients of b_i are defined as

$$b_0 = 2u_1^2 v_1^2 \cos\varphi^{ss} + 2u_1^2 v_1^2 z^2 - (u_1^4 + v_1^4)(1+z^2) \qquad (5.27)$$

$$b_1 = 2(u_1^2 v_1 v_2 + v_1^2 u_1 u_2)[\cos\varphi^{ss} + \cos(\varphi^{ss} - \chi_0)]$$
$$+ 2[(u_1^2 v_1 v_2 + v_1^2 u_1 u_2)z^2 - (u_1^2 u_1 u_2 + v_1^2 v_1 v_2)(1+z^2)](1 + \cos\chi_0) \qquad (5.28)$$

$$b_2 = 2u_1 u_2 v_1 v_2[\cos\varphi^{ss} + 2\cos(\varphi^{ss} - \chi_0) + \cos(\varphi^{ss} - 2\chi_0)]$$
$$+ 2[2u_1 u_2 v_1 v_2 z^2 - (u_1^2 u_2^2 + v_1^2 v_2^2)(1+z^2)](1 + \cos\chi_0) + 2(u_1^2 v_2^2 + u_2^2 v_1^2)\cos(\varphi^{ss} - \chi_0)$$
$$+ 2[u_1^2 v_2^2 + u_2^2 v_1^2]z^2 - (u_1^2 u_2^2 + v_1^2 v_2^2)(1+z^2)\cos\chi_0 \qquad (5.29)$$

$$b_3 = 2(u_2^2 v_1 v_2 + v_2^2 u_1 u_2)\cos(\varphi^{ss} - \chi_0) + \cos(\varphi^{ss} - 2\chi_0)$$
$$+ 2[(u_2^2 v_1 v_2 + v_2^2 u_1 u_2)z^2 + (u_2^2 u_1 u_2 + v_2^2 v_1 v_2)(1+z^2)](1 + \cos\chi_0) \qquad (5.30)$$

and

$$b_4 = 2u_2^2 v_2^2 \cos(\varphi^{ss} - 2\chi_0) + [2u_2^2 v_2^2 z^2 - (u_2^4 + v_2^4)(1+z^2)] \qquad (5.31)$$

Now, I will substitute the expression for the coherence factors for the particle (u_i) and the hole (v_i) into Eq. (5.26). A simpler form of the polynomial equation of Eq. (5.26) may be written as

$$0 = \sum_{i=0}^{4} c_i \left(\frac{\eta}{\sqrt{\delta}} \right)^i \tag{5.32}$$

where the coefficients of c_i are defined as

$$c_0 = \cos \varphi^{ss} + z^2 + E^2(1+z^2) \tag{5.33}$$

$$c_1 = [\cos \phi^{ss} + \cos(\varphi^{ss} - \chi_0) + (1+\cos\chi_0)z^2](E_{+,+} + E_{-,-})$$

$$- [E(E_{+,+} - E_{-,-}) - \sqrt{1-E^2}(E_{-,+} + E_{+,-})(1+z^2)](1+\cos\chi_0) \tag{5.34}$$

$$c_2 = \cos\varphi^{ss} - (1+z^2)(4\cos\chi_0)(\delta E^2 - E_{+,+}E_{-,-})$$

$$+ 2[\cos(\varphi^{ss} - \chi_0) + z^2 \cos\chi_0](1+\delta E^2 + E_{+,+}E_{-,-}) \tag{5.35}$$

$$c_3 = [\cos\varphi^{ss} + \cos(\varphi^{ss} - \chi_0) + (1+\cos\chi_0)z^2 + \cos(\varphi^{ss} - 2\chi_0)](E_{+,+} + E_{-,-})$$

$$+ \delta E(E_{+,+} + E_{-,-}) - \sqrt{1-\delta^2 E^2}(E_{-,+} + E_{+,-})(1+z^2)(1+\cos\chi_0) \tag{5.36}$$

and

$$c_4 = \cos(\varphi^{ss} - 2\chi_0) + z^2 + \delta E - 1 + \delta^2 E^2 \tag{5.37}$$

Here, $\delta = E/\Delta_2$ and

$$E_{\pm,\pm} = \sqrt{1 \pm E}\sqrt{1 \pm \delta E} \tag{5.38}$$

At this stage, I solve Eq. (5.31) numerically to obtain the in-gap bound state energy. The dimensionless parameter z indicates the value of transparency in the junction. For example for $z = 0$, the junction has a high transparency, and the properties of the interface

in the junction is like normal metal. However, increasing z causes the barrier of the junction behaves like an insulator.   For large z, the junction has a low transparency.

5.2 In-gap bound states

As pointed out by Furusaki and Tsukada [10], the mid-gap states in the SIS junction are essential for carrying tunneling currents. The bound states near the energy gap are responsible for the current in the absence of bias voltage (i.e., DC Josephson effect). However, the zero energy bound states are responsible for the current when the bias voltage is applied.

The bound state energy is solved as a function of the band mixing parameter, η. When $\eta = 0$, the two electronic bands are not mixed, indicating that two bands behave as independent of each other. Hence, no interference effect is expected, and the junction behaves as a single-band superconductor Josephson junction. In a single-band case, the result is consistent with the previous result as shown in Fig. 13. In this figure, the bound state energy is shown as a function of φ^{ss}.   I note that φ^{ss} is defined as the phase difference between the s-band condensates in the left and right superconductor island. It seems that, despite the fact that both the left and right superconductor islands in the junction are two-gap superconductors, the junction behaves similar to a junction of two one-gap superconductors. Next, I will numerically solve the secular equation for three different values of z.   For high transparency, the barrier (i.e., $z < 0.01$) seems to behave as a normal metal rather than as an insulator at the interface.   However, when the value of z is increased, the interface behaves more as an insulating barrier.
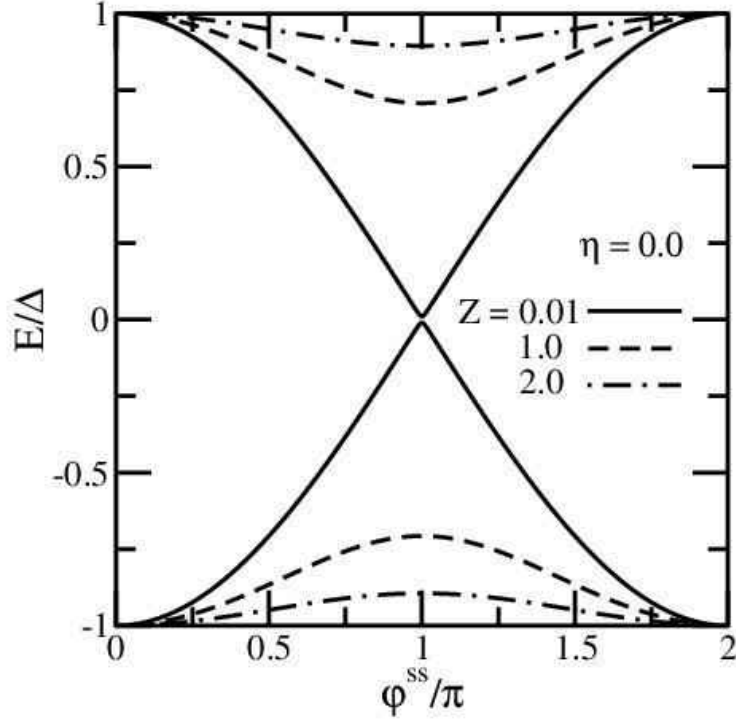
Figure 13: The enegry of bound staes versus phase differnce φ^{ss} to illustrate the energy dispersion. The computed result has been plotted for z = 0.01, 1.0, and 2.0. Here, $\eta=0$, indicating that the junction acts such a two independent one-gap superconductors.

As we note above, when $\eta = 0$ there is no mixing between the wave functions from the two electronic bands, and the junction acts like two separate one-gap superconductor junction (i.e., two independent tunneling channels). On the contrary, when η is non-zero, the band mixing is allowed during the scattering process. The wave function mixing allows for the interference effects. These interference effects may either increase or decrease the supercurrent. So, when the interference effect is destructive, the value of supercurrent will be decrease. The result of numerical calculation for $\eta = 0.2$ shown in Fig. 14 indicates that the bound state energy solution at certain nonzero values of the phase difference φ^{ss}. The bound state energy curves in the figure appear to be shifted compared to those in Fig. 13.
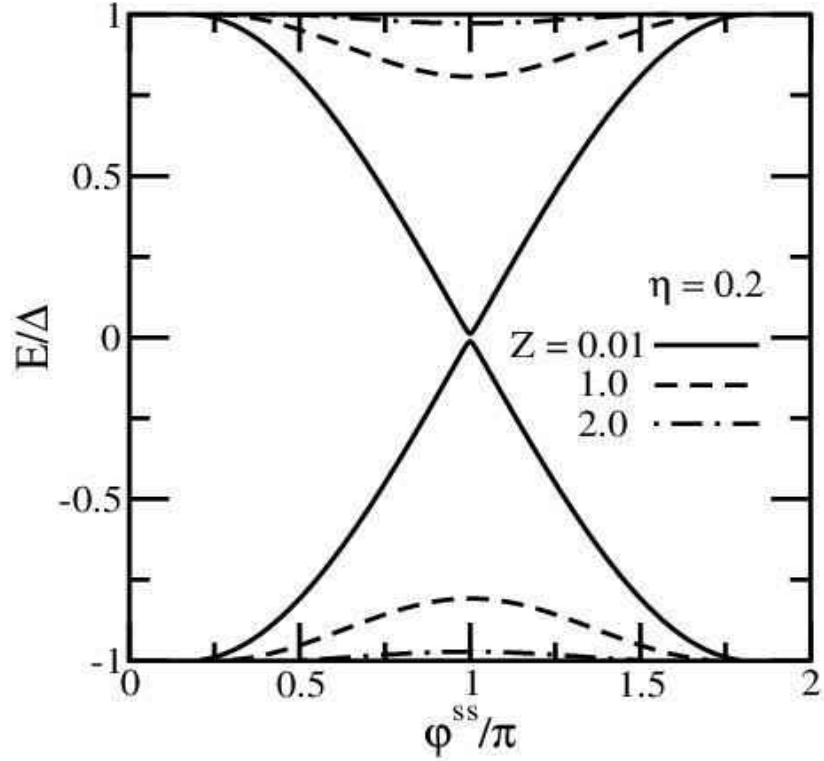
52

Figure 14: The energy of bound states versus phase difference has been illustrated. The energy-phase difference is plotted for $\eta=0.2$ when $z=0.01$, $z=1.0$, and $z=2.0$. The wave function mixing η allows for the interference effects.

Now, I will focus on the mid-gap bound state energy below the Fermi energy. In Fig. 15, I plot the numerically computed bound state energy E_B as a function of the phase difference φ^{ss} for $z = 0.01$ and $z = 1.0$. For each value of z, I plot three curves corresponding to $\eta = 0.0$, 0.1, and 0.2 to illustrate the effects of wave function mixing on the bound state energy. Here, the destructive interference effect due to inter-band interaction appears in the curves for the bound state energy. For both small and large values of the phase difference φ^{ss}, as indicated by the red circles, the interference effects are present. From the results, the destructive interference phenomenon between two wave functions suppresses the bound state energy. When η is small, there is only a small

amount of mixing between two Bloch waves in the two-gap superconductor junction. However, when η increases, the mixing between two Bloch waves leads to increasing either the destructive or constructive interference effect. I note that for a non-zero value of η the bound state energy solution only appears for $\varphi_c^{ss} \leq \varphi^{ss} \leq 2\pi - \varphi_c^{ss}$. Also, I note that the value of φ_c^{ss} increases with increasing z and η. For a large value of z (i.e., z >> 1), the barrier of the junction behaves more like an insulator, rather than a normal metal. The curves show that the bound state energy decreases with increasing z and η.
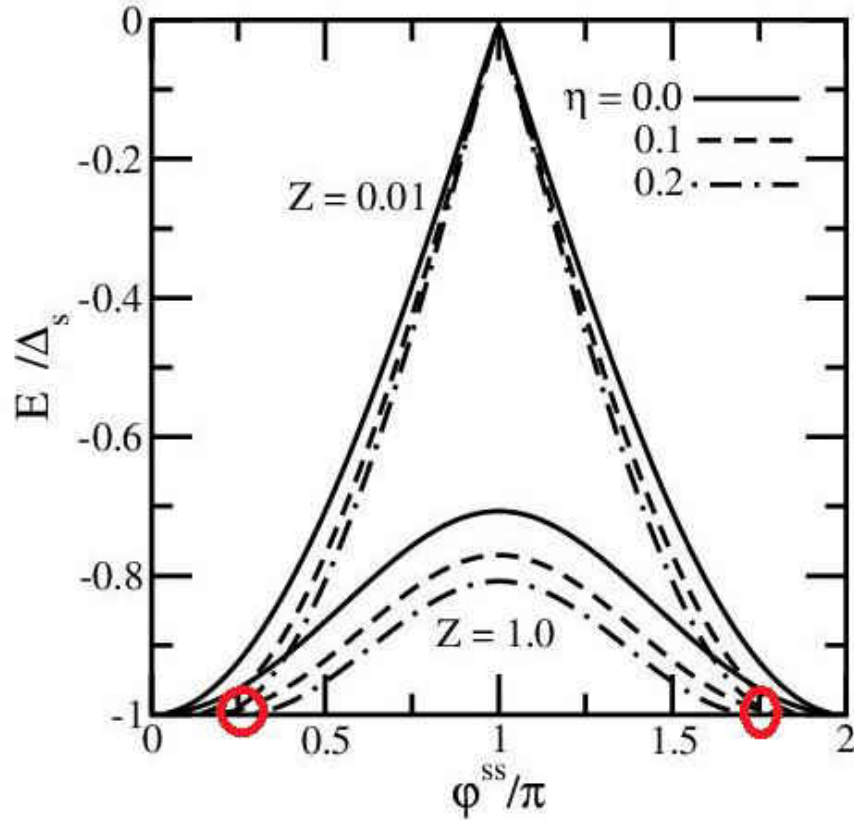

Figure 15: Two sets of curves (i.e., z = 0.01, and 1.0) for the bound state energy versus phase difference are plotted for η = 0.0, 0.1, and 0.2. The destructive interference effect is illustrated with red circles. There is no bound state energy solution in these regions.

5.3 Current-phase relation

In this section, I present the numerically computed supercurrent in the junction as a function of the phase difference φ^{ss}. The current density is given by

$$J_{bound} = \frac{2e}{\hbar} \sum_{n=1}^{2} \frac{\partial E_n}{\partial \varphi^{ss}} f(E_n) \tag{5.39}$$

where

$$f(E_n) = \frac{1}{e^{\frac{E_n(\varphi) - E_F}{k_B T}} + 1} \tag{5.40}$$

is the Fermi-Dirac distribution function. I note that $k_B T \ll \Delta$ in Eq. (5.39) so that the thermal excitations are negligible. According Eq. (5.39), I need to take the derivative of the bound state energy shown in Figs. 14 and 15 numerically with respect to phase difference φ^{ss}.

In Fig. 16, I plot the numerically computed current density from the bound state energy by using Eq. (5.39) as a function of φ^{ss} for $z = 0.01$ and $z = 1.0$ to illustrate the effects of interference. For a small value of potential barrier (i.e., $z \approx 0$), the bound current density, J_{bound}, exhibits both constructive and destructive interference effects. The value of $\varphi^{ss} \approx \pi$, as indicated by the red circle, shows that J_{bound} for $\eta \neq 0$ (i.e., for $\eta = 0.1$ and 0.2) is larger compared to the result of $\eta = 0$ (solid line), suggesting that the interference effect is constructive. However, the curves with small φ^{ss}, as indicated by the blue circle, show that J_{bound} for $\eta \neq 0$ is less than that for $\eta = 0$, suggesting that the interference is destructive. As the barrier potential height z increases, the constructive interference effect for φ^{ss} near π becomes suppressed. However, the curves for small φ^{ss}

indicate that the destructive interference effect becomes enhanced. I note that for a non-zero value of η, the destructive interference effect may completely suppress the bound state current when the barrier potential becomes large.
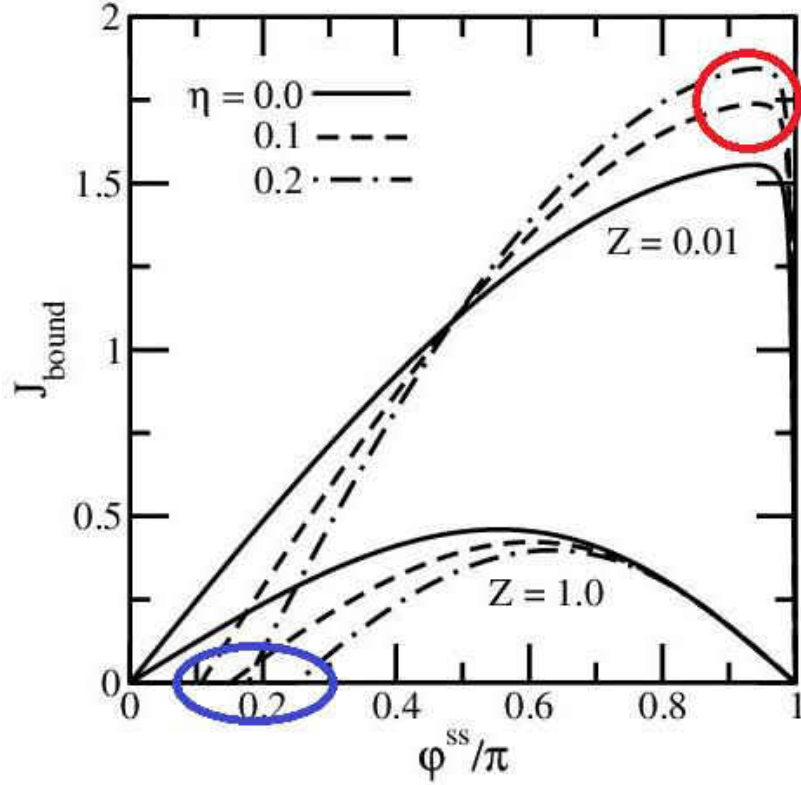

Figure 16: The current density versus phase difference plot for two values for z (z = 0.01, and1.0) illustrates the dependence on the barrier transparency. Three curves for a fixed z correspond to η = 0, 0.1 and 0.2. Constructive interference effect on J_{bound} is indicated by the red circle, but the destructive interference effect on J_{bound} in shown by the blue circle.

In examining Fig. 17, for z = 0.01 and 1.0, the results are not consistent with the well-known current-phase relation of the DC Josephson effect of Eq. (1.2). In the absence of the mixing between two Bloch waves (i.e., η = 0), the usual Josephson current-phase relation is recovered for a large value of z. To illustrate this point, in Fig. 17, I plot $dE/d\varphi$ with respect to the phase difference φ^{ss} for z= 0.5, 1.0, 3.0, and 5.0.

The solid red lines represent the numerically computed J_{bound} from the bound state energy; while the open diamonds represent the Josephson current-phase relation. For a large value of the parameter z, z= 5.0 for example, the two curves become almost identical. This indicates that the Josephson current-phase relation may be derived from the bound state energy solution of Eq. (5.31), as expected.
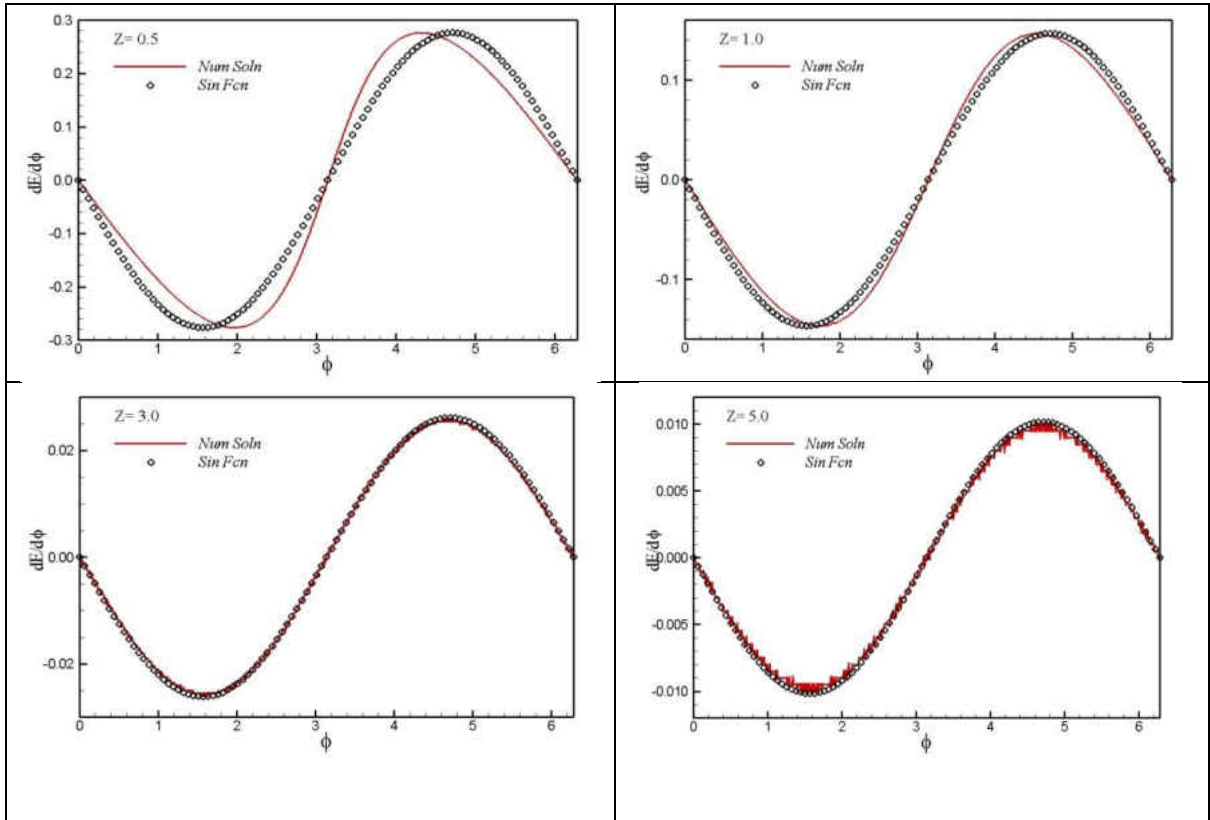

Figure 17: The current density versus phase difference plot for z = 0.5, 1.0, 3.0, and 5.0 illustrate that, when the wave function mixing $\eta = 0$, the current-phase relation becomes more consistent with the usual Josephson relation for one-gap supercurrent with increasing parameter z.

According to curves in Fig. 16, the constructive interference effect for φ^{ss} near π becomes suppressed with increasing z. Now, I plot the maximum value of the bound current density J_{bound}^{max} as a function of z in Fig. 19 to illustrate the crossover behavior.

The curves for $\eta = 0$, 0.1, and 0.2 suggest that the crossover behavior occurs at $z \approx 0.8$. For $z < 0.8$, J^{max}_{bound} becomes stronger with increasing η. This enhancement is due to the constructive interference effect which becomes pronounced for $z \approx 0$ as indicated by the red circle. However, for $z > 0.8$, J^{max}_{bound} becomes suppressed with increasing η. This suppression is due to the destructive interference effect. For $\eta = 0.2$, the destructive interference effect appear to suppress bound state current completely for $z \approx 3$ as shown by the blue circle.
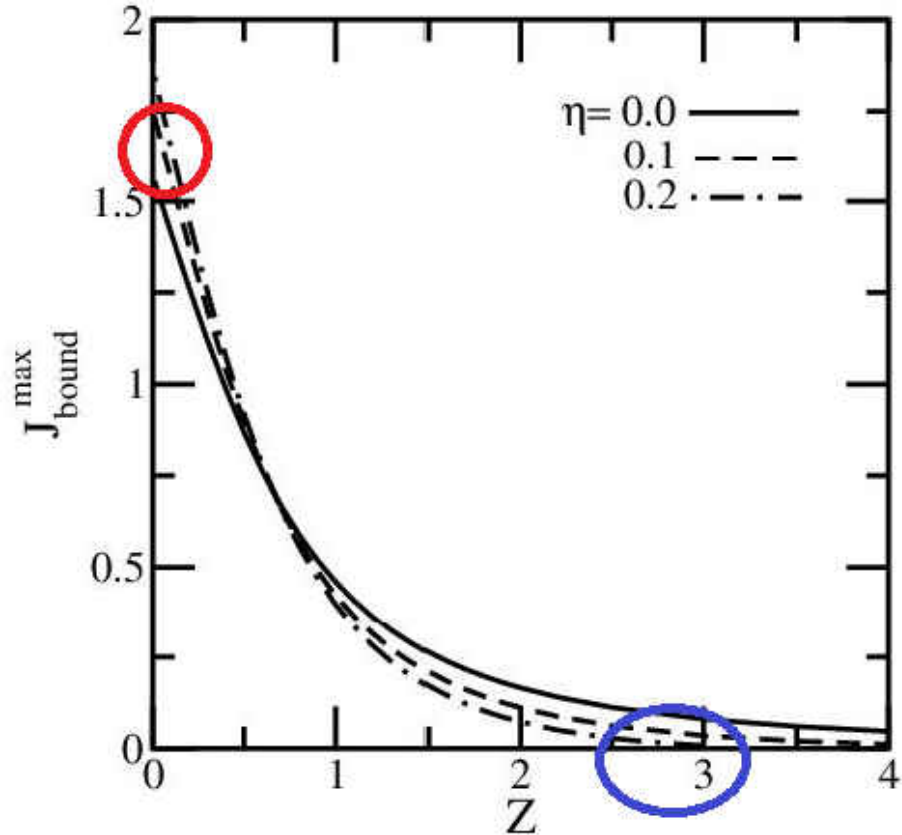

Figure 18: The maximum of current density is plotted as a function of the barrier height z for $\eta = 0.0$, 0.1 and 0.2. The constructive interference effect on the bound states is indicated by the red circle, while the destructive interference effect on the bound states is indicated by the blue circle. At $z \approx 0.8$, the constructive interference effect crosses over to the destructive interference effect. The destructive interference effect suppresses the bound state current completely for $z > 3$.

CHAPTER VI

CONCLUSION

In this thesis work, I have investigated the mid-gap states in two-gap superconductor-insulator-superconductor (SIS) tunnel junction. I studied Andreev bound states in SIS junction by examining a break junction. Here, I used two Bloch waves to construct superconductor wave functions and to investigate the interference effect between the two scattered waves by the barrier potential with an arbitrary barrier transparency. In this thesis work, I obtained the current-phase relation by numerically computing the current density from the mid-gap bound state energy.

In the thesis work, I studied the two-gap superconductor tunnel junction for both when the mixing parameter η is zero and when it is non-zero. When $\eta = 0$, the Bloch waves of two-gap superconductors do not interfere. Therefore, the two-gap superconductor junction behaves as a one-gap superconductor junction with two independent tunneling channels. On the other hand, when the band mixing is allowed (i.e., $\eta \neq 0$) during the tunneling process, destructive inter-band interference would prevent a formation of mid-gap bound states for certain ranges of the phase difference φ^{ss}. I found that when the mixing between two Bloch waves is increased, the interference effect becomes stronger. In short, either the destructive or constructive interference becomes stronger.

My thesis work shows that when the barrier of the junction behaves an insulator for large z, the usual current-phase relation is recovered. The result of current density calculation shows that for small value of transparency (i.e., $z \approx 0$), the maximum value of the bound state current density J_{bound}^{max} increases with increasing η. The bound current density J_{bound} exhibits both the constructive and destructive interference effect. The numerical result for this case shows that the bound state energy decreases with increasing both z and η.

As shown in the present thesis work, the current-phase relation for a SIS break junction may use as a way to measure the amount of band mixing in a tunneling process. Consequently, the unusual dependence of the tunneling current on φ^{ss} may arise, indicating the presence of bound states only in the limited range of the phase difference. This work may be taken as a starting point for further research work on the role of the wave function interference in the property of tunnel junctions involving multi-component superconductors.

REFERENCES

1. M. Tinkham, *Introduction to Superconductivity* (Dover Publications, New York, 2004).

2. C. J. Gorter and H. Casimir, *The Cold Wars: A History of Superconductivity* (Rutgers University Press, New Jersey, 2003) p307.

3. J. Bardeen, L. N. Cooper, and J. R. Schrieffer, Phys. Rev. **108**, 1175 (1957).

4. A. Markelz, S. Whitmore, J. Hillebrecht, and R. Birge, Phys. Med. Biol. **47,** 3797 (2002).

5. K. J. Seibert, T. Loffler, H. Quast, M. Thomson, T. Bauer, R. Leonhardt, S. Czasch, and H. G. Roskos, Phys. Med. Biol. **47**, 3743 (2002).

6. A. J. Fitzgerald, E. Berry, N. N. Zinov'ev, S. Homer–Vanniasinkam, R. E. Miles, J. M. Chamberlain, and M. A. Smith, J. Biol. Phys. **29,** 123 (2003).

7. R. M. Woodward, V. P. Wallace, R. J. Pye, B. E. Cole, D. D. Arnone, E. H. Linfield, and M. Pepper, J. Investigative Dermatol. **120**, 72 (2003).

8. C. Kittel, *Introduction to Solid State Physics* (John Wiley & Sons, New York 1996) p366.

9. G. E. Blonder, M. Tinkham, and T.M. Klapwijk, Phys. Rev, B **25**, 4515 (1982).

10. A. Furusaki and M. Tsukada, Phys. Rev. B **43**, 10164 (1991).

11. J. Chen, J. L. Zhang, L. Jiao, Y. Chen, L. Yang, M. Nicklas, F. Steglich, and H. Q. Yuan, New J. Phys. **15**, 053005 (2013).

12. Yu. A. Nefyodov, A. M. Shuvaev, and M. R. Trunin, EPL **72**, 638 (2005).

13. Ya. G. Ponomarev, S. A. Kuzmichev, M. G. Mikheev, M. V. Sudakova, S. N. Tchesnokov, T. E. Shanygina, O. S. Volkova, A. N. Vasiliev, and Th. Wolf, Zh. Eksp. Teor. Fiz. **140**, 527 (2011) [JETP **113**, 459 (2011)].

14. Y. Nakajima, G. J. Li, and T. Tamegai, Physica C **468**, 1138 (2008).

15. Y. Bugoslavsky, Y. Miyoshi, G. K. Perkins, A. V. Berenov, Z. Lockman, J. L. MacManus Driscoll, L. F. Cohen, A. D. Caplin, Supercond. Sci. Tech. **15**, 526 (2002).

16. F. Bouquet, R. A. Fisher, N. E. Phillips, D. G. Hinks, and J. D. Jorgensen, Phys. Rev. B **87**, 047001 (2001).

17. F. Bouquet, Y.Wang, I. Sheikin, T. Plackowski, and A. Junod, Phys. Rev. B **89**, 257001 (2002).

18. X. K. Chen, M. J. Konstantinović, J. C. Irwin, D. D. Lawrie, and J. P. Franck, Phys. Rev. Lett. **87**, 157002 (2001).

19. X. Xu, W. Li, X. Wang, and S. X. Dou, *Superconducting Properties of Graphene Doped Magnesium Diboride* (University of Wollongong, Australia, 2011) p202.

20. P. Samuely, P. Szabo, J. Kacmarcik, T. Klein, and A. G. M. Jansen, Physica C **385**, 244 (2004).

21. T. Dahm, *Frontiers in Superconducting Materials* (Springer, Berlin, 2005).

22. Y. Bugoslavsky, Y. Miyoshi, G. K. Perkins, A. D. Caplin, and L. F. Cohen, Phys. Rev. B **69**, 132508 (2004).

23. Y. Kamihara, T. Watanabe, M. Hirano, and H. Hosono, J. Am. Chem. Soc. **130**, 3296 (2008).

24. R. S. Gonnelli, D. Daghero, M. Tortello, G. A. Ummarino, V. A. Stepanov, R. K. Kremer, J. S. Kim, N. D. Zhigadlo, and J. Karpinski, Physica C **469**, 512 (2009).

25. H. Suhl, B. T. Matthias, and L. R. Walker, Phys. Rev. Lett. **3**, 552 (1959).

26. S.-Z. Lin, Phys. Rev. B **86**, 014510 (2012).

27. Y. Tanaka, Phys. Rev. Lett. **88**, 017002 (2002).

28. Y. Ota, M. Machinda, and T. Koyama, Phys. Rev. B **83**, 060503(R) (2011).

29. J. H. Kim, B.R. Ghimire, and H. Y. Tsai, Phys. Rev. B **85**, 134511 (2012).

30. T. Dahm, *Frontiers in Superconducting Materials* (Springer, Berlin, 2005).

31. X. Y. Feng and T. K. Ng, Phys. Rev. Lett. **79**, 18503 (2009).

32. A. A. Golubov, A. Brinkman, Y. Tanaka, I. I. Mazin, and O.V. Dolgov , Phys. Rev. Lett. **103**, 077003 (2009).

33. T. K. Ng and N. Nagaosa, EPL **87**, 17003 (2009).

34. Michael L. Edgar and Jonas Zmuidzinas, Airborne Telescope Systems, Proc. of SPIE, **4014** (2000).

35. R. C. Jaklevic, J. Lambe, A. H. Silver, and J. E. Mercereau, Phys. Rev. Lett. **12**, 159 (1964).